Operations Research Forum _####################_
https://doi.org/10.1007/s43069-025-00495-0

RESEARCH

Atrous Convolution-Based Adaptive 3D-CNN Model for Breast Cancer Diagnosis Using Segmentation in Mammogram Images

Rashmi V Pawar[1] · Rajashekhargouda C. Patil[2] · Rajeshwari S. Patil[3] · Ambaji S. Jadhav[1]

Received: 26 September 2024 / Accepted: 13 June 2025
© The Author(s), under exclusive licence to Springer Nature Switzerland AG 2025

For Approval

Abstract

A commonly affected disease for women is breast cancer, caused by abnormal growth of the breast tissues. Existing breast cancer detection approaches rely on manual segmentation, which consumes more time and is ineffective for handling variations in breast tissue density and texture. Moreover, these methods often fail to detect subtle abnormalities, leading to missed diagnoses. Additionally, they are vulnerable to overfitting, lack robustness to noise and artifacts, and require extensive computational resources. To overcome these challenges, a novel deep learning-based framework for breast cancer detection using mammogram images has been introduced. At first, the necessary images are collected from online sources. The mammogram image is subjected to the preprocessing approach via contrast-limited adaptive histogram equalization (CLAHE) and histogram equalization (HE) to obtain a high-contrast image with reduced noise. Consequently, the pre-processed image is fed to the hybridization of Improved UNet-FCN for segmenting the image over cancer-occurred regions. The parameters within the segmentation are optimized by the farmland fertility snow leopard optimization (FFSLO). After, the segmented image is given to the breast cancer detection stage. Here, the atrous convolution-based adaptive 3D-convolutional neural network (AC-A3DCNN) is utilized to detect breast cancer. Here, the variable tuning is carried out with the FFSLO to boost the demonstrated approach's detection accuracy rate. While validating the statistical test, the designed model shows 2.61%, 2.05%, 4.86%, and 0.68% elevated than CHOA, CMO, FFOA, and SNOA for best metrics. Hence, the offered approach's efficacy is revealed through the comparative evaluation of the diverse baseline models concerning the standard performance measures.

Keywords Breast cancer detection · Histogram equalization · Contrast limited adaptive histogram equalization · Farmland fertility snow leopard optimization · Atrous convolution-based adaptive 3D-convolutional neural network · UNet and fully convolutional network

Extended author information available on the last page of the article

1 Introduction

Women are easily affected by breast cancer in recent days, so detecting breast cancer is important to survive their life [1]. Moreover, the final stage of this disease may lead to sarcoma. Hence, early-stage detection is very important. To detect this breast cancer, hospitals and clinics utilize a variety of images such as MRI scans, ultrasound scans, CT scans, and mammograms [2]. The image-based techniques provide high-resolution images and hence it is helpful to detect abnormal tissues present in the breasts [3]. In a mammography image, the blood tissues are often represented as a collection of coefficients or intensities, which includes fatty and thick glandular tissues [4]. The greatest markers of this disease's existence can be noticed on mammography, and the tissues with unclear masses can be labeled as abnormal growth [5]. In the world, there is a high level of knowledge among the younger generations, and detection is much easier with mammogram images [6]. There are a lot of quality screening methods presented in breast cancer detection in these mammograms, which increased the need for computer-aided methods for effectively detecting breast cancer [7]. A pathology diagnosis is often the best standard for identifying breast cancer. The excised tissue is analyzed in the lab before being subjected to imaging processes [8]. The staining procedure frequently involves using hematoxylin and eosin (H&E). Two methods are developed for this analysis, genomics and histopathological image analysis [9]. Histopathological images are said to be microscopic images, and the microscopic images with breast tissues are very helpful in the early stage of cancer detection.

Multi-level oblique (MLO) mammography is a kind that records the texture of the breast tissue in a specific location [10]. Using established methods like Otsu, local thresholding, segmentation, and clustering, the exact location of the tissues is identified. With the usage of bi-level color in the suggested approach, thresholding is the process of turning a specific image with a grayscale or RGB into an image with less intensity [11]. The thresholding approach is the foundation of Otsu's clustering [12]. The image with a threshold includes a few groups of pixels or bi-modal, and this algorithm attempts to choose the best threshold value to divide into two classes of images [13]. Edge detection can be done using techniques such as Laplacian, Sobel, and Roberts's edge operators. Using the graph cut approach, the provided chunk and sub-portion of coefficients are categorized into a better region based on a predetermined criterion [14]. This method simply starts with a collection of points at the beginning, and the region is expanded by finding the nearest coefficient.

Radiologists should use computer-aided diagnostic (CAD) technologies to identify and delineate the boundaries of breast cancers. Many researchers have recently been presented to increase breast mass classification performance by using deep representations of breast images [15]. Additionally, it is challenging for the radiologist to identify the molecular subtypes on mammographic images. Recently, excellent accuracy was achieved by classifying molecular subtypes using texture patches taken from mammography via a convolutional neural network (CNN) [16]. As a result, several researchers have tried to define breast cancer molecular subtypes using the morphological information of tumor shape [17, 18].

FOR APPROVAL

The Motivation of the Proposed Method The existing model can effectively detect breast cancer. However, they often suffer from low accuracy, variability, and artifacts in cancer detection. Moreover, they have limitations in handling complex and heterogeneous breast cancer data, and they have struggled to detect diseases at the initial stage The existing methods have difficulty in analyzing breast cancer's molecular subtypes from mammograms. Additionally, they require a more number of input data for an effective detection process and suffer from generalization capability. All these challenges motivate to develop an innovative deep structured-aided detection model.

Significance of the Designed Framework in Overcoming the Existing Problems The challenges faced by the existing models are effectively overcome by leveraging an innovative hybrid framework that merges the power of UNet-FCN-based segmentation and 3DCNN-based classification. This approach enables the precise detection and segmentation of breast tumors, even in the presence of noise and variability. Moreover, the developed model utilizes a hybrid algorithm named FFLSO, which incorporates the strength of FFOA and SLOA to improve detection accuracy. Additionally, the parameters of the proposed method are optimized using the FFLSO algorithm, which can effectively enhance the generalizability of the approach. The combination of UNet and FCN in the segmentation process can effectively reduce the need for more data, resulting in improved performance and robustness in breast cancer detection. The designed framework effectively overcomes the challenges faced by existing approaches and provides a more reliable solution.

The contributions of the newly promoted deep structured-aided detection of breast cancer systems are discussed here:

- To adopt an effective deep structured-based breast cancer detection approach for supporting women to detect abnormal changes in the breast tissues in the early stage. The efficacy of the offered approach is applicable to real-time applications.
- To design an efficient pre-processing model to boost the contrast of the gathered image and reduce the unwanted noise from the collected images using HE and CLAHE techniques. It is utilized to ignore the irrelevant portion of the images and also helps to attain a better-resolution image.
- To develop an effective FFSLO method for optimizing the parameters like activation function, epochs in the UNet-based segmentation, and the momentum and epochs in FCN and also the epochs in the AC-A3DCNN to increase the accuracy rate of the designed model.
- To design an effective segmentation model to segment the pre-processed images using hybridization of the UNet-FCN method via the developed FFSLO to obtain the segmented images to identify the tissues in the images effectively. Epochs and momentum parameters in the hybrid segmentation process are optimized to improve the segmentation performance.
- To implement an effective detection framework to detect the tumor using the AC-A3DCNN method. Here, the epochs in the developed classifier are optimized using the developed FFSLO to improve the detection accuracy. The optimization of the offered approach is utilized to reduce the overfitting issues and computation time.

For Approval

Organization of the Manuscript The residual of this work is adapted to organize the developed deep structured-aided breast cancer detection model and is explained as follows. The previous techniques illustrate breast cancer detection, and the advantages and disadvantages are also presented in Sect. 1. The gathered mammographic datasets, the illustration of sample images, and the structural representation of the offered approach is provided. It summarizes the hybrid heuristic algorithms presented in the optimization section and explains the segmentation process based on UNet and FCN. It describes the developed AC-A3DCNN model for the classification of tumors. The experimental setup and the implementation outcome are given in Sect. 3. The discussion and conclusion of the suggested deep structured-aided tumor diagnosis technique are summarized in Sect. 4 and Sect. 5.

1.1 Literature Review

In 2022, Su et al. [19] developed a double-shot technique for simultaneous segmentation and mass detection. The final segmentation choice was then created by combining the two branches. Two different mammography datasets were taken to evaluate the suggested YOLO-LOGO model. The suggested model outperformed well compared to the other existing approach.

In 2021, Punithavathi et al. [20] introduced mammography images using the optimized kernel fuzzy clustering algorithm to detect breast cancer. The hybrid denoising filter (HDF) approach provided a noise-free image using the suggested segmentation algorithm. Data clustering made it easier to combine comparable data and dissimilar data types separately. The outcome demonstrated that the offered system was more accurate than the well-known K-means, kernel fuzzy clustering algorithm (KFCA), and Otsu techniques.

In 2021, Keshk et al. [21] presented a pre-trained architecture where the features were retrieved utilizing a CNN. The suggested model performance has been assessed using six metrics, including precision, specificity, sensitivity, ROC curve (AUC), F1-score, and accuracy. The developed classification method was given high precision, sensitivity, specificity, AUC, F-score, and accuracy. The tenfold cross-validation technique experimental findings have demonstrated the effectiveness of the TL of the VGG16 technique as higher than in other techniques.

In 2016, Cascio et al. [22] recommended the ROI Hunter method for locating masses in mammograms. The MAGIC-5 collaboration database included 3762 digital images taken at various hospitals. By using a segmentation method and the ROI Hunter technique, it was possible to reduce the size of the whole image under examination without losing any important details. The subsequent classification stage involved extracting features, which was crucial since some characteristics supplied geometrical information and others shaped attributes. Whether the ROI is pathogenic or not is determined by the output neuron. Results were presented based on FROC and ROC curves. This program was a part of the CAD station at the MAGIC-5 Collaboration Hospitals.

In 2020, Shen et al. [23] suggested a combined classification and segmentation of benign and malignant lesions utilizing mixed supervision and a UNet approach. The method effectively segmented the tumor regions to project a discerning map to

For Approval

classify the malignant and benign tumors simultaneously. It has been done by coupling a strong supervision segmentation mask and weak supervision with a benign-malignant label through a straightforward annotation scheme. By adding the balance segments and the SegNet design, this network, known as ResCUNet, expanded UNet to better use multilevel information for tissue identification. They tested the effectiveness of the suggested strategy on a public mammography database from INbreast, and they consistently outperformed the leading algorithms.

In 2020, Kumar et al. [24] presented a novel framework to segment a breast tumor. The resulting masks were also divided into four different tumor formations using shape descriptors like lobular, round, oval, and irregular on a CNN. The suggested model produced higher accuracy than the conventional techniques.

In 2020, Nagalakshmi et al. [25] demonstrated a deep CNN (DCNN) that improved the accuracy of classifying breast cancers from mammography images by utilizing the K-means multiclass support vector machine technique and clustering. There are two stages to the segmentation process. The object was included in various region-of-interests that were first created using the input images. After the bounding box regions were adjusted and a coefficient-range mask was made for the entity, the object class was predicted in the secondary phase. These two distinct stages were connected to the DCNN pyramidal hierarchical structure, which extracted features from the images. At last, the findings of the simulations showed that the EnsembleNet outperformed the traditional classifiers.

In 2019, Punitha et al. [26] offered a fuzzy rough set theory (FRST) to create a tumor classification technique in mammography images, and it provided an accurate way of texture and feature extraction. The main goal of installing FRST was the feature extraction procedure, which was accomplished by employing a rapid reduction method that aids in quickly identifying the tumor without pixel loss. The mammography image was subjected to fuzzy-rough instance selection (FRIS), which was then combined with the fuzzy-rough nearest neighbor (FRNN) approach for segmentation. The findings produced using the suggested approaches were compared by diverse performance metrics, including exact calculations for accuracy, sensitivity, and specificity.

Moreover, a multi-core support vector machine (SVM) model [27] has been proposed for an effective prediction process. This technique supports clinical practices and patient care. Furthermore, a cutting-edge-based deep learning model [28] has been designed to detect breast tumors. This technique attained notable performance in terms of accuracy. Additionally, a deep learning model [29] was introduced for the medical image classification. This approach can effectively reduce the annotation costs, particularly in complex images. For the prognosis and robust characterization of breast cancer, a deep transfer learning approach [30] was introduced. This process reduces the pathologist's strain by analyzing the mammography images of patients. Furthermore, a deep CNN-based approach [31] effectively classifies the Breast lesions in mammographic images. This technique helps the clinician with effective treatment planning. The hybrid deep neural network-based approach [32] was suggested for diagnosing cancerous polyps. In addition, deep learning schemes [33] were designed to diagnose breast cancer. These models effectively detect breast cancer; still, they consume more time to detect the cancer accurately. Therefore, an innovative deep learning-based breast cancer detection model was designed in this work.

For Approval

1.2 Problem Description

Mammography is the widely utilized procedure for effectively identifying breast cancer detective diseases. Breast tumor recognition at the premature stage using a mammographic image is more complicated. Hence, automatic detection systems are required to identify breast cancer with reduced time, computational cost, and decreased cost requirements.

- While segmenting the images, the conventional approaches accomplished low performance in the localization process and also needed to speed up the training process to reduce latency. Therefore, this has to be solved by utilizing the hybridized deep learning models.
- While detecting breast cancer diseases, most of the existing approaches decrease the overfitting problem and also cannot detect diseases at the initial stage which can affect the complexity of the system. Consequently, it is required to utilize advanced deep-structured approaches to resolve these issues.
- The mobility of the existing approaches is high. Here, mobility refers to the model is very sensitive to small variations in the data, leading to inconsistent predictions and potentially high false positive rates. Moreover, image resolution is poor in the baseline models, which reduces the precision performance. Therefore, this has to be solved by using hybridized heuristic algorithms to enhance the accuracy and precision rate.
- The conventional approaches need more training of the classifiers while identifying the tissues in the images, and the confidentiality of the model is very low. The generalization capability is high, and also it requires enormous input data for effective detection. Therefore, it is essential to use more advanced techniques for detecting breast cancer diseases in the starting stage.

However, these disadvantages are resolved using the newly proposed deep learning-based breast cancer disease diagnosis approach.

For Approval

2 Materials and Methods

2.1 Developed Breast Cancer Diagnosis Model

Breast cancer is the most severe health issue in the entire globe. Computer-aided detection, Mammography, breast MRI, and ultrasound are some of the breast cancer screening tools that are extremely receptive in medical research. With the assistance of the output, an image generated by these approaches, the doctor can analyze and even diagnose the tumors. Despite being a useful screening tool, mammography does not offer accurate and trustworthy performance for women with thick breasts or those undergoing surgery. Recent studies have demonstrated that because MRI does not expose patients to radiation, it is a better option than mammography. Breast MRI primarily contains some challenges. Screening high-risk women was advised due to the interpretations

like complexity and limited specificity. Therefore, a new deep structured-aided breast cancer detection method is proposed to deliver superior real-time disease detection services. The architectural depiction of the introduced system is given in Fig. 1.

The proposed FFSLO-AC-A3DCNN is used to detect the changes in breast tissues. The input gathered images are collected from online resources. Next, the processing is applied to the images using histogram equalization and CLAHE techniques. Then, the preprocessed images are taken by the segmentation model. In the segmenting section, the images are segmented individually by UNet and FCN methods. "The activation function and the epochs in the UNet and the momentum and the epochs in the FCN are optimized with the implemented FFSLO." The resultant FCN and UNet-based segmented images are averaged to get the output image. The optimization of parameters in the segmentation process will help to improve the segmentation process. Next, the final segmented images are given in the last section. Here, the convolutional-based AC-A3DCNN detection is used to detect the tissues in the segmented images. The parameters present within the AC-A3DCNN are tuned using the offered FFSLO to maximize accuracy. Then, the test results of this proposed detection model are compared to other techniques for validating the performance by various evaluation measures.

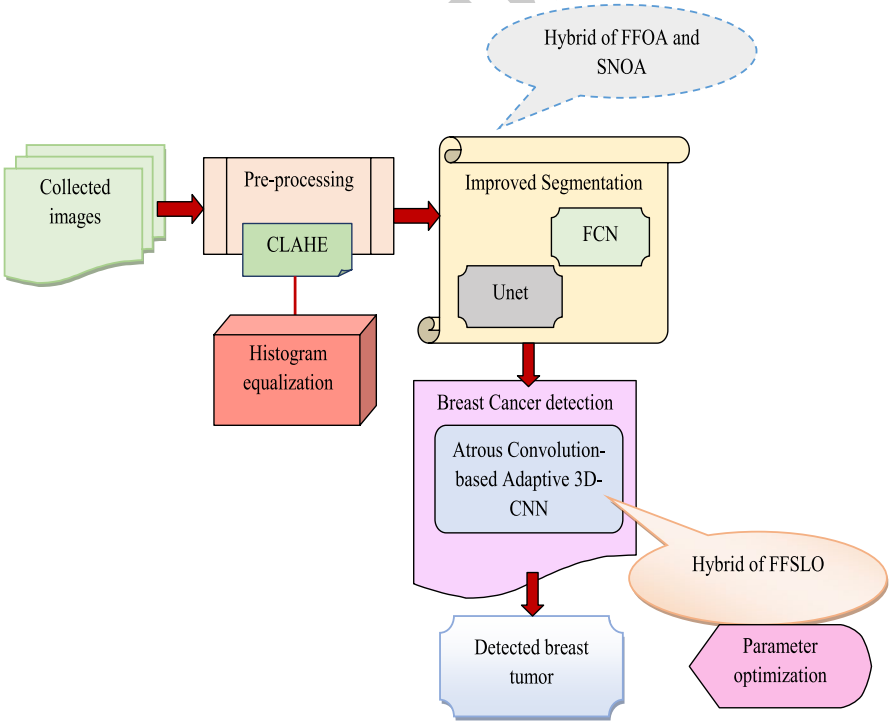

Fig. 1 Architectural representation of the developed model

2.2 Mammogram Breast Cancer Datasets

The images required for the offered approach are collected from the following benchmark datasets.

In Dataset 1 (MIAS Mammography) The wanted images to be garnered from the external source link is "https://www.kaggle.com/datasets/kmader/mias-mammography: access date: 2022–11-02." The mammography scan dataset with breast images is presented in online resources, and it is accessible to everyone. Totally, 327 files are presented in the MIAS dataset. The all-mias, info.txt, all_mias_scans.h5 folders are placed in this dataset. The benign and malignant are found using this dataset. Some classes are ASYM, NORM, SPIC, CIRC, CALC, ARCH, and MISC, which are placed in the third column.

In Dataset 2 (CBIS-DDSM: Breast Cancer Image Dataset) The required images are garnered from the link "https://www.kaggle.com/datasets/awsaf49/cbis-ddsm-breast-cancer-image-dataset: access date: 2025–02–10." The dataset files are in Jpeg format. The size of the dataset is 6.3 GB with 10.2 k files. It contains 6 CSV files.

To deal with a class imbalance issue, data augmentation is used in the developed model. The data augmentation addresses class imbalance by artificially generating new data points, primarily for the minority class. This process can effectively increase the data size and allow the approach to learn more efficiently from underrepresented categories. The sample images and augmented images are shown in Fig. 2. The term WA_{CL}^{HS} and CL = 1,2, ..., A are represented as collected input images. Here, A is the number of images in the database.

2.3 Mammogram Pre-processing Phase

Images are used for model training and inference. Before that, they undergo image preprocessing. The preprocessing procedure is quite helpful for removing the errors, noises, and outlines that are present in the images. Utilizing preprocessing methods improves the final performance of the detection of breast cancer models. This developed model uses the HE and CLAHE algorithms in this preprocessing section. The term WA_{cl}^{HS} is an input image of the preprocessing method.

Reason for Choosing the HE and CLAHE Technique Pre-processing plays an important role in the mammogram image. It helps to reduce the background noises of the medical data to improve the image quality, and it enhances the reliability. Several pre-processing mechanisms have been utilized in recent years; yet, it faces several challenges. In the conventional wavelet transform [34], it does not perfectly clean the noisy medical data to enhance negative outcomes in the segmentation performance, leading to higher mortality rates. It is not capable of optimally capturing the subtle differences in the mammogram images, and it needs additional processing measurements to clean the gathered data. The existing median filtering [35] takes more

For Approval

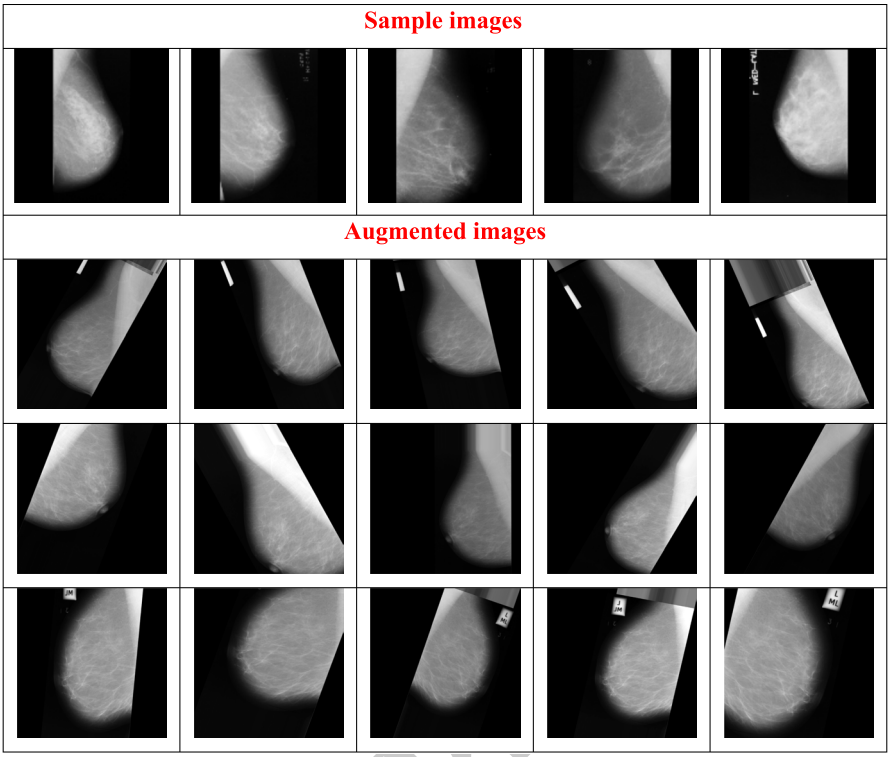

Fig. 2 Sample images and augmented images

duration in the preprocessing phase to minimize the overall segmentation performance. Also, it generates more false positive and false negative outcomes to reduce the earlier diagnosis. Furthermore, it is not capable of dealing with vast amounts of high-resolution images, maximizing the overfitting and underfitting issues. Considering the traditional anisotropic diffusion filter [36], it is too complex for minimizing the artifacts and irrelevant content in the gathered data, reducing the image quality. Also, it can minimize the convergence speed and interpretability of the segmentation process. Therefore, the HE and CLAHE are utilized in this research work to optimally enhance the pre-processing phase for improving image quality. The HE mechanism can effectively capture the background noise and artifacts in both bright and dark regions. It has the ability to handle low contrast, poor lighting, and narrow-range medical mammography images for improving the image quality. This helps to reduce the misclassified and negative outcomes, leading to better segmentation. Additionally, the CLAHE mechanism can reveal fine details of edges in the images, especially in subtle variations. This can lead to better diagnosis and treatment in earlier stages for protecting human life. It needs minimal computational duration to identify the background noises in an effective manner. The HE and CLAHE have faster computation and simpler implementation than the conventional pre-processing frameworks. Thus, the effectiveness of HE and CLAHE make them suitable as

For Ap

preprocessing steps for improving image quality to enhance the breast cancer diagnosis in a timely manner.

The developed model employed HE and CLAHE to enhance image contrast and uniformize the distribution of grayscale values. HE was specifically mentioned as useful for enhancing low-contrast mammograms by equalizing pixel intensity distributions. CLAHE further focused on local contrast enhancement and minimized over-amplification of noise by working on small image tiles and blending neighboring regions with bilinear interpolation. HE adjusts the pixel values to create a uniform histogram and helps to enhance the overall contrast in an image, while CLAHE adapts local regions to preserve details and reduce noise in the image. Due to this process, the proposed system can deal with the variation in image quality and effectively address the low-quality issue. So, these techniques are chosen in the developed model for improving contrast and reducing noise.

Histogram Equalization[37] The input image is given to the breast cancer diagnosis model preprocessing section WA_{CL}^{HS}. Histogram equalization [38] is used for improving image contrast and has previously been successful. HE [39] is a technique that uniformizes an image's distribution of grayscale values. The inverse transformation q can be restored t, as shown in Eq. (1).

$$q = U^{-1}(t) \tag{1}$$

$$L_0 = rond\left(\frac{D_j(2^S - 1)}{X, z}\right) \tag{2}$$

This technique is especially helpful for images with foreground and background or dark or black. The outcome attained after the HE procedure is noted by the term WA_{CL}^{OS}.

CLAHE The input data given in the CLAHE method is WA_{CL}^{OS}. CLAHE [40] operates on a tiny part of the image, called tiles, as opposed to the histogram equalization approach, which operates directly on the entire image. As a result, image analysis techniques are required to delineate and identify breast cancers because they accurately depict the vital morphological data required for a valid diagnosis. The output data present after the CLAHE method is WA_{CL}^{PO}.

For Approval

2.4 Developed FFSLO

The offered FFSLO is promoted to maximize the accuracy rate of the deep structured-aided detection of breast cancer approach. Therefore, utilizing this hybrid optimization approach greatly enhances the efficacy of the offered model.

Reason for Choosing the FFSLO Algorithm Over the Other Optimization Algorithms The developed FFSLO algorithm effectively outperformed existing optimization techniques, such as genetic algorithms (GA) [41], particle swarm optimization (PSO) [42], whale optimization algorithm (WOA) [43], and ant colony optimization

(ACO) [44]. The GA and ACO often suffer from early convergence, which leads to attaining suboptimal solutions in disease detection. Moreover, PSO has slow convergence. Furthermore, WOA is sensitive to parameter settings and requires careful tuning. This may lead to time-consuming and computationally expensive processes. In contrast, the developed FFSLO model utilizes the strength of FFOA and SLOA optimization, allowing the FFSLO algorithm to effectively explore the solution space, which can lead to avoiding premature convergence and help achieve optimal solutions in disease diagnosis. Furthermore, the exploration and exploitation capabilities of the FFSLO algorithm can avoid getting stuck in a local optima and allow careful tuning. Finally, the FFSLO algorithm provides a more effective and efficient solution for optimizing complex problems. So, this algorithm is chosen for optimizing the parameters in UNet-FCN and AC-A3DCNN during breast cancer detection.

Discussion on How the FFOA and SLOA Elements Relate to One Another The FFOA and SLOA elements are connected to each other to form the proposed FFSLO framework. These elements leverage their respective strengths to achieve an efficient and effective FFSLO algorithm. Here, the FFOA element is employed to explore the solution space, utilizing its unique farmland fertility-inspired mechanism. This mechanism can effectively help to identify promising regions and avoid local optima. As the FFOA algorithm converges to a promising region, the SLOA element is implemented to refine the search and then converge to optimal solutions. The SLOA's snow leopard-inspired behavior can effectively avoid the local optima and converge to the global optimum. The exploration and exploitation abilities of the FFOA and SLOA allow the FFSLO framework to adaptively adjust its search strategy based on the problem's requirements. By integrating the FFOA and SLOA elements, the FFSLO framework improved its efficiency in breast cancer detection.

Novelty Using this designed FFSLO, the "epochs and the activation function in UNet and the momentum and the epochs in the FCN are tuned and also the epochs in the detection classifier are tuned" to improve the detection performance. FFOA[29] has proven to be an effective heuristic algorithm for issues with lower dimensions, and it has nicely optimized the problems. The amount of dimensions considerably reduces the effectiveness of other algorithms, and FFOA yields better results. The SLOA[30] is significantly more competitive than similar algorithms because it can deliver more accurate solutions. However, these algorithms do not find clean alternative sources of energy or cost-effective and reliable functions. Consequently, the FFOA and SLOA algorithms are integrated to boost the classification stage accuracy. The whole process in the proposed model is a parameter belonging to mating that occurs with probability in the FFSLO, and it is indicated by w. If the value of probability is $w > 0.5$, the position of the FFOA method is selected. Otherwise, the position of the SLOA method is selected. Equation (3) is used to estimate the parameter w.

$$w = \frac{q + \beta}{\sqrt{t} + \alpha} \tag{3}$$

For Approval

Hyperparameter Tuning Process of the Designed FFSLO Algorithm The FFSLO algorithm is used to tune the parameters like activation function, epochs in the UNet-based segmentation, and the momentum and epochs in FCN and also the epochs in the AC-A3DCNN to enhance its performance in the breast cancer detection model. At first, the FFSLO algorithm initializes the population solutions, where each solution represents a unique combination of hyperparameters in the UNet-FCN and adaptive 3D-CNN model. Furthermore, the fitness of each solution was evaluated using the validation set and then the FFSLO algorithm performed selection, crossover, and mutation operators to the population to generate new offspring. The population was updated with the new offspring, and this process was repeated for a specified number of iterations. Finally, the optimal solution was selected based on the highest fitness value, representing the best combination of hyperparameters. Through this process, the FFSLO algorithm optimizes hyperparameters within specific ranges that can maximize the accuracy of the breast cancer detection model. This parameter-tuning process played an essential role in preventing overfitting by selecting the most optimal hyperparameters for model training. The detailed description of the conventional FFOA and SLOA are described below.

Conventional FFOA[45] The FFA optimization method concept is based on assessing the soil's quality in each location of farmland. Therefore, Farmers employ a variety of products to enhance the quality of farmland. The principal ways to find the finest materials and products for enhancing soil quality are characterized as follows:

- *The first stage*: Population initialization

This initial step in generating the entire population A is described by Eq. (4).

$$A = L * O \tag{4}$$

Here L is a positive integer that is bigger than 0. The search space is divided using the constant L. The term O is an integer. It lists the options for each search space potential solution.

$$Y_{kl} = M_l + rnd(0,1) \times (u_l - l_l) \tag{5}$$

The size of RES plants is indicated by Y. The first stage creates a random solution between upper and lower bounds variables that are u_l and l_l, respectively.

- *Second stage*: Determine the quality of the soil

Here, the following Eq. (6) can be used to assess the soil quality of each portion of farmland.

$$\mathrm{Sec}_t = Y(bl), b = o^*(t-1) : o^*tt = \{1,2,...P\}, l = \{1,2,...,4\} \tag{6}$$

For Approval

The quality of farmland is assessed using the average value of the current solutions and measured using Eq. (7). Then, every part solution is also calculated.

$$\mathrm{Sec}_r = Y(bl), b = o^*(r-1) : o^*rr = \{1,2,...P\}, l = \{1,2,...,4\} \tag{7}$$

- *Third stage*: Update the memories

Here, Eq. (8) and Eq. (9) are the best global memory and best local memory calculated, respectively.

$$N_{loc} = rond(u * o), \quad 0.1 < u < 1 \tag{8}$$

$$N_{Global} = rond(u * o), \quad 0.1 < u < 1 \tag{9}$$

Here, the term N_{Global} indicates how many solutions are kept in the global memory. Then the term N_{loc} is the number of the solutions that are kept in the local memory. At last, this section updates both memories.

- *The fourth stage*: The quality of soil changing

The soil quality of each segment has been calculated by Eq. (10). The best and worst solutions are combined using Eq. (10) and (11).

$$I = \beta * rnd(-1,1) \tag{10}$$

$$Y_{new} = I * \left(Y_{kl} - Y_{N_{Global}}\right) + Y_{kl} \tag{11}$$

The random solution is indicated by $Y_{N_{Global}}$ and the term Y_{kl} is represented as the worst part of farmland. Then the new solution is denoted by Y_{new}. The decimal number is denoted by I and it is derived from Eq. (12).

$$I = \delta * rnd(0,1) \tag{12}$$

$$Y_{new} = I * \left(Y_{kl} - Y_{ul}\right) + Y_{kl} \tag{13}$$

Here, the random solution is represented by Y_{ul}. After updating the solutions, the combination solutions are measured using Eq. (12) and Eq. (13).

- *Fifth stage*: A combination of soil

Farmers combine each soil in the final step using the best options stored in the local memory of each part inside the areas used for farming.

For Approval

$$H = \begin{cases} Y_{new} = Y_{kl} + \lambda_1 * \left(Y_{kl} - B_{Global}(c)\right) & R > rnd \\ Y_{new} = Y_{kl} + rnd(0,1) * \left(Y_{kl} - B_{local}(c)\right) & else \end{cases} \tag{14}$$

The terms B_{local} and B_{Global} are indicated by the combination solutions, and it is calculated by Eq. (8) and Eq. (9), respectively.

$$\lambda_1 = \lambda_1 * S_w,\ 0 < S_w < 1 \tag{15}$$

The parameter R, which must be changed at the beginning of the optimization method, ranges from 0 to 1. Finally, a new solution Y_{new} is created following the changes that have been made.

- *The sixth stage*: Final solutions

The current options in the search area are assessed using the objective function.

$$H = \begin{cases} Y_{new} = Y_{kl} + \lambda_1 * \left(Y_{kl} - B_{Global}(c)\right) & R > rnd \\ Y_{new} = Y_{kl} + rnd(0,1) * \left(Y_{kl} - B_{local}(c)\right) + \left(Y_{kl} - Y_{N_{Global}}\right) & else \end{cases} \tag{16}$$

A 'random solution based on the best solution in the local memory and the best global solution' from the previous iteration is given in Eq. (17).

$$\lambda_1 = \lambda_1 * S_w,\ \ 0 < S_w < 1 \tag{17}$$

The updated segment is indicated by Y_{kl}. The finest option for global memory is B_{Global}. The best solution for local memory is B_{local}.The term $Y_{N_{Global}}$ is one of the global memories of existing random solutions.

Conventional SLOA[46] Each snow leopard is included in the suggested SLOA. Members of the SLOA include snow leopards who work as search agents.

- *Phase 1*: Movement and travel routes

Additionally, snow leopards move in indirect lines in a zigzag style. Equation (18) and Eq. (19) represent the stage of the suggested SLOA mathematically.

$$\begin{aligned} y_{j,e}^{Q1} &= y_{j,e} + s \times \left(y_{m,e} - J \times y_{j,e}\right) \times sign\left(G_j - G_m\right), \\ m &\in 1,2,3,...,P,\ e = 1,2,3,....,n \end{aligned} \tag{18}$$

$$Y_j = \begin{cases} y_j^{Q1}, & G_j^{Q1} < G_j \\ y_j, & else \end{cases} \tag{19}$$

For Approval

The "term y_j^{Q1} is the updated location of e^{th} the snow leopard based on phase j^{th} and the objective function value G_j^{Q1}", and random number r in the range of [0, 1].

$$K = rond(1 + v) \tag{20}$$

A term m is a selected snow leopard's row number. Then the 'term $y_{j,e}^{Q1}$ is the novel rate for e^{th} the problem variable attained by j^{th} the snow leopard in the phase e^{th}.

- *Phase 2*: Hunting

The behavior of snow leopards when attacking prey and hunting is employed in the second step. Equation (21) and (22) are used to simulate the snow leopards' natural hunting behavior.

$$Q_{j,e} = y_{j,e}, \ e = 1, 2, 3, ..., n \tag{21}$$

Equation (23) represents the approach of a snow leopard. The parameter Q is the proportion of the prey distance.

$$y_{j,e}^{Q2} = y_{j,e} + s \times \left(\left(Q_{j,e} - y_{j,e}\right) \times Q + \left(Q_{j,e} - 2 \times y_{j,e}\right) \times (1 - Q)\right) \times sign\left(G_j - G_m\right) \tag{22}$$

$$Y_j = \begin{cases} y_j^{Q2} & G_j^{Q2} < G_j \\ Y_j & else \end{cases} \tag{23}$$

Here, the value of the SLOA taken in the observation is 0.375.

- *Phase 3*: Reproduction

At this stage, the snow leopards' normal reproductive habits, a new half of the overall worth of additional individuals are added to the algorithm's population. The snow leopard reproductive process is involved in Eq. (24) based on the aforementioned mathematical models.

$$D_m = \frac{y_m + Y_{P-1+1}}{2} \tag{24}$$

The term D_m is the m^{th} cub between two snow leopards.

- *Phase 4*: Mortality

Snow leopards with lower objective functions are more likely to pass away. Algorithm 1 shows the pseudocode for the FFSLO algorithm.

For Approval

Algorithm 1 Designed FFSLO

Input: Parameters like activation function and epochs in the UNet, the momentum and epochs in FCN and also the epochs in the AC-A3DCNN
Output: Optimal parameters like activation function and epochs in the UNet, the momentum and epochs in FCN and also the epochs in the AC-A3DCNN
1. Initialize the number of populations
2. Set the maximum number of iterations
3. Update the variable w
4. Set the parameter w **with the adaptive concept in Eq. (3).**
5. Estimate the fitness function
6. **For** $t = 1 to M_{iter}$
7. **For** $j = 1 to N_{Po}$
8. **If** $w > 0.5$
9. Update the FFOA algorithm
10. **Else**
11. Update the SNOA algorithm
12. **End if**
13. Verify the fitness function
14. **End for**
15. **End for**
16. Update the new position
17. **Get the best solution**
18. **End**

For Review

2.5 UNet Segmentation

Image segmentation is frequently adopted to identify boundaries in images and objects.

UNet[47] The Unet-based breast segmentation architecture contains seven dropout layers. The activation function leaky ReLU is also used here. Assume a softmax as an activation function, 1×1 as a convolution filter and it is given a 3-channel gray-level output map. The term $S = \left(S^1, S^2, S^3\right)$ is a prediction vector. The training time values are set to S^1 is 0 S^2 is 0.5 and S^3 is 1 and these values are said to be gray-level prediction values.

Loss Function The batch size is indicated by K and the entropy information of each coefficient is determined by given Eq. (25).

$$\mathrm{KRC} = -\frac{1}{K}\sum_{j=1}^{K} C + C^{`} \tag{25}$$

The term $C^{`} = \sum_{R=1}^{3}\left(1 - z^{(R)}\right).\log\left(1 - S^{(R)}\right).z^{(R)}$ is an actual value and the term $C = \sum_{R=1}^{3} z^{(R)}$ is information entropy. Here, the mini-batch serial number is denoted by j. The updated binary-cross-entropy function is calculated by Eq. (26).

$$\mathrm{FRC}(z) = -\frac{1}{K}\sum\nolimits_{j=1}^{K}\sum\nolimits_{R=1}^{3}\left[z_j^{(R)}.log\left(S_j^{(R)}\right) + \left(1 - z_j^{(R)}\right).log\left(1 - S_j^{(R)}\right)\right] \tag{26}$$

The probability loss of the coefficient channel is given in Eq. (27).

$$\mathrm{LoSS} = -z^{(R)}.logS^{(R)} - \left(1 - z^{(R)}\right)log\left(1 - S^{(R)}\right) \tag{27}$$

The value of R is set to be $R = 1, 2, 3$. The training section contains three various gray-level probability values and three different gray-level prediction values.

2.6 FCN Segmentation

The input is to be given to the FCN-based segmentation process. The size of each layer of data in a convent is $i \times a \times e$ and d is the channel dimension. The color channels d and pixels with a size of $i \times a$ is the first layer. Higher layer locations match the areas in the image to which they are path-connected or what is referred to as their receptive fields. These functions calculate outputs z_{ab} for the data vector at the position (a, b) and it is given in Eq. (28).

$$z_{ab} = h_{mn}\left(\left\{Y_{rj+\varphi j+ri+\varphi i}\right\}0 \le \varphi i, \varphi j \le m\right) \tag{28}$$

Translation invariance is the foundation of convnets. Their fundamental parts need relative spatial coordinates and work on local input areas. Here, the deep filter or fully connected network computes the nonlinear filter. In this work, the FCN performs as an input and the respected output as spatial dimensions.

The kernel size is indicated by m and the strider sub-sampling factor is characterized by n. The term h_{mn} explains the layer types, such as an element-wise nonlinearity layer, spatial max pooling, and matrix multiplication for convolution or average pooling. The stride obeying the transformation rule is given in Eq. (29).

$$i_{mn} \circ om^{`}n^{`} = (i \circ g)m^{`} + (m-1)n^{`}, nn^{`} \tag{29}$$

The real-valued function is determined using the term $\beta(y, \lambda) = \sum_{mn} p^{`}\left(y_{mn}, \lambda\right)$. The λ value is a whole image of the decent gradient value. While an all-purpose deep network determines an all-purpose nonlinear position, a network with only these layers calculates a completely convolutional network, also known as a deep

For Approval

filter, which is a nonlinear filter. An FCN naturally runs on any size input and generates a commensurate output.

2.7 Improved UNet-FCN-based Tumor Segmentation

The developed segmentation process utilizes UNet and FCN with parameter optimization for providing accurate results over the segmentation process. The UNet and FCN segmentation performs with very few training samples and gives high performance after segmenting the images. UNet and FCN segmentation contain some drawbacks, such as high noise sensitivity in the breast cancer detection model. So, the improved UNet-FCN-based tumor segmentation was added to the offered detection of breast cancer model.

Novelty Initially, the preprocessed images WA_{CL}^{OS} subjected to the UNet-FCN-based segmentation method. This technique leverages the strength of UNet and FCN. Here, UNet and FCN receive the pre-processed images initially to perform the process. The UNet contains two sections which are the decoder and the encoder. These two encoders repeat the same 3×3 convolution layers. The encoder performs a down-sampling, which is used for reducing the spatial dimension and increasing the feature channels. The decoder performs an up-sampling and it is adapted for restoring the details. The UNet-based segmentation output is AS_{U}^{OG}.The FCN in the segmentation process helps to precisely segment each pixel in an image to its corresponding class. Here, the FCN architecture enables them to process images of any size without the need for fixed input dimensions. The FCN module further refines the segmentation results, producing a more accurate and detailed representation of the tumor region. The FCN-based segmentation output is AS_{M}^{FN}.

The segmentation process is further optimized using the FFSLO algorithm, which tunes the parameters like activation function and epochs in the UNet, the momentum and epochs in FCN, and also the epochs in the AC-A3DCNN. The features extracted by both UNet and FCN modules are averaged to create the final segmented image. The resultant UNet-based segmented images $f1$, and FCN-based segmented images $f2$, create the final segmented image. This averaging process enables the fusion of the complementary strengths of both architectures, resulting in a highly accurate and robust segmentation result SN_{o}^{RO}. Equation (30) provides the averaging process to obtain the final segmented image output.

$$SN_{o}^{RO} = avg(f1, f2) \tag{30}$$

The final output of the UNet-FCN segmentation process is used for further analysis and diagnosis.

Trade-Off Between Accuracy and Interpretability The combination of UNet and FCN in the developed model can effectively balance the trade-off between accuracy and interpretability. UNet incorporates skip connections, allowing the model to preserve spatial information from earlier layers, which is crucial for precise segmentation. By upsampling features from the encoder during the decoding process, UNet

For Approval

can better capture fine details within the image. This may lead to achieving high accuracy in segmentation tasks. Furthermore, FCNs tend to be more interpretable because of their simpler architecture, making it easier to visualize the attribute maps generated at the diverse phases of the network. By leveraging the strength of UNet and FCN in the segmentation process, the developed model can effectively trade off the accuracy and interpretability in breast cancer detection.

Performance of UNet-FCN-based Tumor Segmentation Compared to Other Architectures The proposed UNet-FCN model averages the outputs of UNet and FCN leading to superior performance compared to various segmentation techniques, like mask region-based convolutional neural network (R-CNN) [48], UNet [49], FCN [50], SegNet [51], and DeepLab [52]. The Mask R-CNN is a popular segmentation architecture that depends on region proposal networks (RPNs) to generate proposals. This can lead to errors in cases where proposals do not accurately capture objects of interest. Furthermore, UNet can suffer from limited contextual information, while FCN can struggle with spatial details. Moreover, SegNet and DeepLab may not arrest the specific characteristics of images, leading to suboptimal presentation in the detection process. However, the proposed UNet-FCN model directly predicts segmentation masks without relying on proposals. By averaging the outputs of UNet and FCN, the proposed model can capture both contextual information and spatial details, making it a more robust and accurate segmentation technique. Furthermore, the proposed model's ability to average outputs from multiple models can capture the specific characteristics of medical images, enabling it to reduce overfitting. Finally, the proposed model's unique approach to averaging outputs from UNet and FCN enables it to outperform various segmentation techniques.

2.8 3D-CNN Model

The 3DCNN [53] outperforms the other neural network methods for static and hybrid motion and characteristics, and also, the 3DCNN achieves the best precision. In recent years, a popular method has been used for classifying data in the neural network design related to 3D convolution layers. The 3DCNN architecture is frequently used for moving 3D objects, particularly in medical imaging. The kernel values directions are (a, b, s) given in Eq. (31).

$$w_{kl}^{abs} = \tanh\langle Y_{kl} + \sum\nolimits_{n} \sum_{e=0}^{E_k-1} \sum_{f=0}^{F_k-1} \sum_{g=0}^{G_k-1} z_{k\ln}^{efg} w_{\langle k-1\rangle n}^{\langle a+e\rangle\langle b+f\rangle\langle c+g\rangle} \tag{31}$$

Here, the term w_{kl}^{abs} is the kernel value in the preceding layer. Three-dimensional volume space represents the output shape.

2.9 Atrous Convolution-Based Adaptive 3D-CNN Model

We suggest using a method known as 3D atrous convolution to capture both the spatial and temporal information in an image. The encoder and decoder models

For Approval

are effective in segmentation, but the different combinations of max pooling layers reduce the feature maps' spatial resolution. To overcome this issue, an atrous convolutional-based adaptive 3DCNN model is developed.

Novelty The segmented images SN_o^{RO} are fed into the 3D-CNN of the developed AC-A3DCNN model. The 3D-CNN architecture is performed using a three-dimensional filter to extract spatial hierarchies and characteristics from the segmented image. This is particularly useful, where the 3DCNN can effectively analyze moving 3D objects. However, 3D-CNN reduces the spatial dimensions of the feature maps, decreasing the resolution. So, the atrous convolution is added to the 3D-CNN. The utilization of atrous convolution plays a pivotal role in capturing both spatial and temporal information in an image without reducing the resolution. By incorporating atrous convolutional into the adaptive 3D-CNN architecture, the introduced framework can effectively address the issue of reduced spatial resolution caused by max-pooling layers in traditional encoder-decoder architectures. The atrous convolutional helps to control the dilation rate, which determines the spacing between the weights of the convolutional filter. By adjusting the atrous rate, the model can confine multi-scale contextual information from the inputted image. The atrous rate (t, s) (e, f, g) on the l^{th} feature map in the K^{th} layer is $z_{k\ln}^{efg}$, and it is determined using Eq. (32).

$$z_{k\ln}^{efg} = \mathrm{Re}LU\left(C_{kl} + \psi\right) \tag{32}$$

$$\psi = \sum_{n} \sum_{e=0}^{E_k-1} \sum_{f=0}^{F_k-1} \sum_{g=0}^{G_k-1} z_{k\ln}^{efg} w_{\langle(k-1)\rangle n}^{\langle a+e\times t\rangle\langle b+f\times t\rangle\langle s+g\times r\rangle} \tag{33}$$

The rectifier function is represented by ReLU, and the term C_{kl} is a feature map of l^{th} position. Then the term $(k-1)$ is an overall feature map that is placed in K^{th} position. Moreover, the parameters of AC-A3DCNN are tuned using the algorithm to maximize the accuracy of the breast cancer detection system. Finally, AC-A3DCNN offers the detected breast cancer outcome.

The newly implemented optimization process's objective function is to maximize the breast cancer detection system accuracy, and it is calculated using δL as given in Eq. (34).

$$\delta L = \underset{\left\{Eo_s^{AR}, Ms_n^{YK}, Eo_u^{GL}, AF_j^{TR}\right\}}{\arg\min} \left(\frac{1}{Ac}\right) \tag{34}$$

Here, the term Eo_s^{AR} is the optimized epoch in the UNet in the interval of [50 , 100] and the term Ms_n^{YK} is the optimized epoch in the FCN in the interval of [50 , 100]. The term Eo_u^{GL} is the optimized activation function in the UNet in the range between [0 , 4] and the term AF_j^{TR} is the optimized momentum in the FCN in the range between [0.01 , 0.99]. The term ACC is represented as accuracy. The negative and positive samples are utilized to determine the accuracy and it is given in Eq. (35).

$$Accuracy = \frac{(TP + TN)}{(TP + TN + FP + FN)} \tag{35}$$

For Approval

The atrous convolution is an alternative layer for the down-sampling layer in the 3DCNN model. The epochs in the atrous convolution-based adaptive 3D-CNN are [1000, 5000].

Adaptation of 3D-CNN to 2D Mammograms and its Advantages The adaptation of 3D-CNN to 2D mammograms helps to accommodate the unique characteristics of 2D mammographic images. By treating the 2D image as a single slice within a 3D volume, the adapted 3D-CNN architecture was able to process 2D images while leveraging the benefits of 3D-CNN. This adaptation helps the architecture to capture more complex features and patterns in 2D mammograms, which is crucial for accurate image analysis and diagnosis of breast cancer. Compared to traditional 2D-CNNs, the 3D-CNN architecture offered significant advantages in breast cancer diagnosis. The 2D CNN architecture is limited in understanding the spatial relationships for complex scenes. Additionally, 2D CNNs require more training data to reach optimal performance, require high computational costs, and also may suffer from overfitting issues. These limitations are effectively tackled by the developed 3D-CNN architecture. The 3D-CNN architecture has the ability to capture larger receptive fields for a better understanding of spatial relationships and contextual information. Furthermore, this architecture provides better generalization capabilities to new, unseen data, which is essential for applying the model to diverse patient populations. The adaptation of 3D-CNN helps the developed model to achieve accurate performance compared to traditional 2D CNNs.

For Approval

3 Calculation of Results

3.1 Simulation Setup

Python was used to develop a deep learning-based breast cancer identification model. The usefulness of the newly developed FFSLO-AC-A3DCNN-based breast cancer detection model was then validated by conducting this experiment using various performance measures. A population size of 10 should be used, and a chromosomal length of 5 was necessary for diagnosing a variety of cancers. Furthermore, this type of breast cancer detection could only use a maximum of 25 iterations. The algorithms that should be taken for the comparison were the chimp optimization algorithm (CHOA) [54], continuous media optimization (CMO) [55], FFOA [45], and SNOA [46]. For this comparison analysis, techniques like CNN [21], UNET [47], DCNN [25], and 3DCNN [53] were used for computation. Accordingly, a variety of assessment metrics such as FDR, FPR, precision, sensitivity, MCC, accuracy, FNR, F1-score, and specificity have been taken for the comparison.

3.2 Evaluation Measures

The performance measures used for the developed system are described below.

(a) False negative rate (FNR): FNR is calculated as the ratio of actual breast cancer cases misclassified as non-cancerous.

$$FNR = \frac{FN}{FN + TP} \tag{36}$$

(b) Sensitivity: The sensitivity is estimated by the proportion of actual breast cancer cases correctly classified as cancerous and presented in Eq. (37).

$$Sensitivity = \frac{TP}{TP + FN} \tag{37}$$

(c) Precision: The overall numbers of positive samples are counted in Eq. (38). Also, it computes the ratio of positive breast cancer cases to all cases in the sample.

$$precision = \frac{TP}{TP + FP} \tag{38}$$

(d) Negative predictive value (NPV): It is a proportion of predicted non-cancerous cases that are actually non-cancerous, and it is computed using Eq. (39).

$$NPV = \frac{FP}{FN + FP} \tag{39}$$

(e) F1-score: In the implemented detection model, the F1-score value is related to the average precision and recall values.

$$F1score = \frac{2 * TP}{2 * (TP + FP + FN)} \tag{40}$$

(f) Matthews correlation coefficient (MCC): It measures the correlation between predicted and actual breast cancer classes.

$$MCC = \frac{TP \times TN - FP \times FN}{\sqrt{(TP + FP)(TP + FN)(TN + FP)(TN + FN)}} \tag{41}$$

(g) Specificity: Eq. (42) is used to compute the specificity of the developed detection technique based on negative samples.

$$Specificity = \frac{TN}{TN + FP} \tag{42}$$

(h) False positive rate (FPR): It is a proportion of predicted cancerous cases that are actually non-cancerous, and it is signified in Eq. (43).

$$FPR = \frac{FP}{FP + TN} \tag{43}$$

For Approval

(i) False discovery rate (FDR): The proportion of false values to all positive samples is given in Eq. (44).

$$FDR = \frac{FP}{FP + TP} \tag{44}$$

Here, the term *TP* indicates the true positive, *TN* defines the true negative, *FN* represents the false negative, and *FP* denotes the false positive, respectively.

3.3 Evaluation Analysis of Various Methods and Algorithms Over the Cancer Breast Detection Model

The effectiveness of the offered approach is contrasted with different algorithms that are shown in Fig. 3 (a), and also different breast cancer identification techniques are given in Fig. 3 (b). This analysis is done by using various metrics and allows the researchers to understand how the developed method achieved specific goals in breast cancer detection. The implemented FFSLO-AC-A3DCNN-based breast cancer detection model has greater precision of 34.16%, 44.7%, 50.4%, and 61.3% when compared to various methods like CNN, UNET, DCNN, and 3DCNN, and the learning percentage is 50. By taking into all of the performance indicators, the designed FFSLO-AC-A3DCNN-based breast cancer detection model achieved more efficacy than the other methods. Moreover, the developed model can effectively identify and delineate the boundaries of objects within an image and enables timely intervention and treatment, increasing the survival rates of patients.

3.4 K-fold Analysis of Various Methods and Algorithms Over the Recommended Model

The efficacy of the offered model over diverse heuristic algorithms is exposed in Fig. 4 and presented in Fig. 5 compared to other breast cancer detection methodologies. This analysis assesses the stability of a model's performance across different data splits, providing a more robust evaluation of its generalization ability. Concerning the K-fold strategy value of 3, the implemented model has more precision of 24%, 2.4%, 3.0%, and 3.8% than CNN, UNet, DCNN, and 3DCNN various methods. The new breast cancer identification model outperforms the heuristic algorithms and the current breast cancer detection methodologies' accuracy. Moreover, the result demonstrated that optimizing the parameters in the offered approach can accurately identify breast cancer at a premature stage.

3.5 The Overall Analysis of the Offered Framework

The newly developed FFSLO-AC-A3DCNN system is validated using several heuristic algorithms and conventional methods of the cancer detection model. Table 2 compares the model's performance using various detection

For Approval

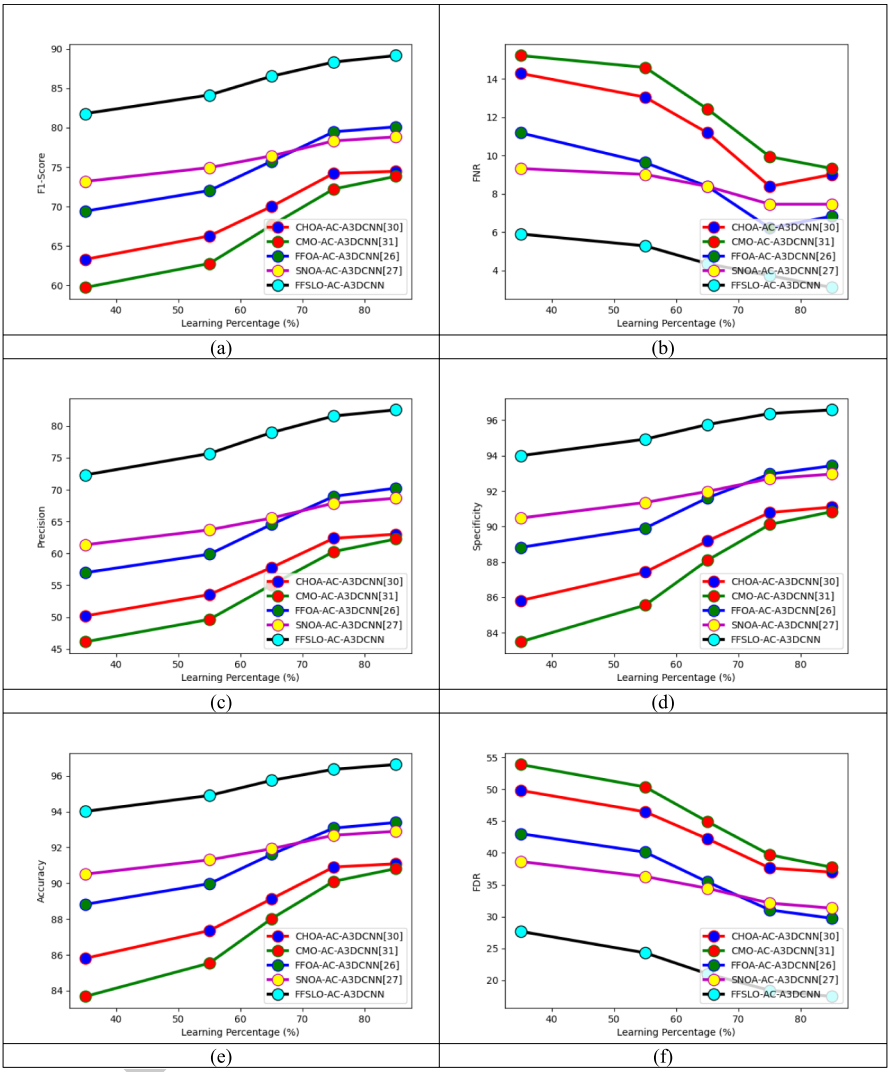

Fig. 3 **a** The evaluation of the implemented framework over different heuristic algorithms in regards to a F1-score; b FNR; c precision; d specificity; e accuracy; f FDR; g FPR; h sensitivity; i MCC; j NPV. **b** The evaluation of the implemented framework over different detection techniques in regards to **a** F1-score; **b** FNR; **c** MCC; **d** precision; **e** specificity; **f** accuracy; **g** FDR; **h** FPR; **i** NPV; **j** sensitivity

methodologies and heuristic algorithms. The developed cancer detection model's effectiveness over the various algorithms is in Table 1. Additionally, Table 2 compares the developed model's effectiveness over the already-used techniques. According to this investigation, the suggested cancer detection model assured precision improvements of 30.9% compared to CHOA-AC-A3DCNN, 32.5% compared to CMO-AC-A3DCNN, 17.4% compared to FFOA-AC-A3DCNN, and 20.1% compared to SNOA-AC-A3DCNN cancer detection models. Also, the

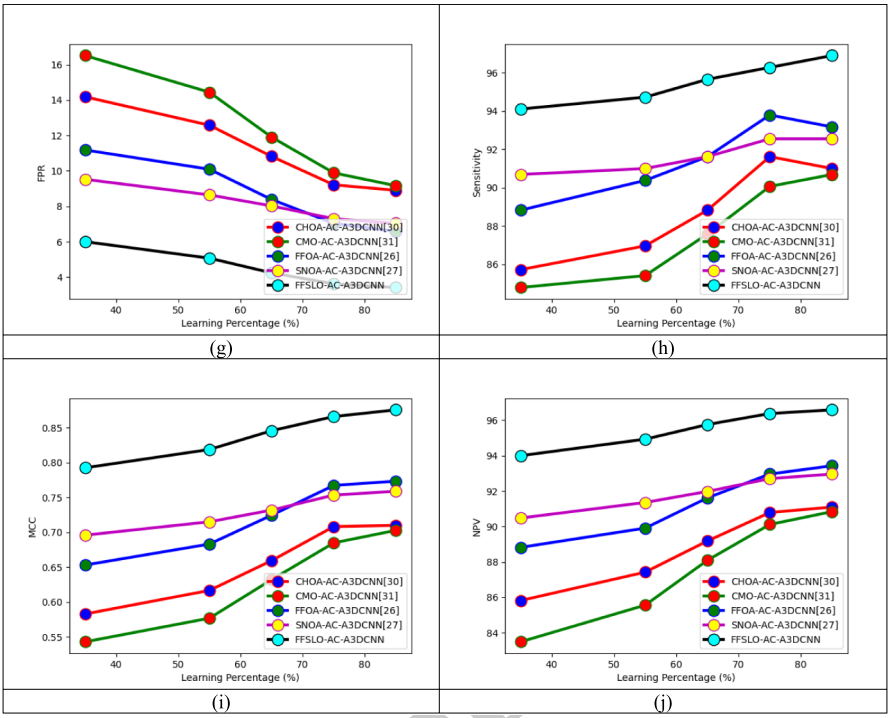

Fig. 3 (continued)

designed approach would give higher performance than other methods. Moreover, the outcome showed that the FSLO algorithm in the developed model can potentially reduce false negatives, assisting doctors in detecting tumour more accurately.

3.6 Validation of the Designed Model Using Recent Techniques

The validation of the designed framework is shown in Table 3. The results show that the offered approach attains better results than the other recent techniques. The precision of the designed model is 96.63%. Thus, the outcome demonstrated that the developed model can identify potential signs of breast cancer in medical imaging, like mammograms. Moreover, it proved that the combination of UNet and FCN in the proposed framework can effectively analyze the patterns and features of the image, allowing for earlier breast cancer detection.

3.7 Statistical Validation of the Designed Approach Using Friedman Aligned Ranks Test

The statistical validation of the offered approach using the hypothesis test is shown in Tables 4 and 5. It is the non-parametric option to the one-way analysis

For Appr

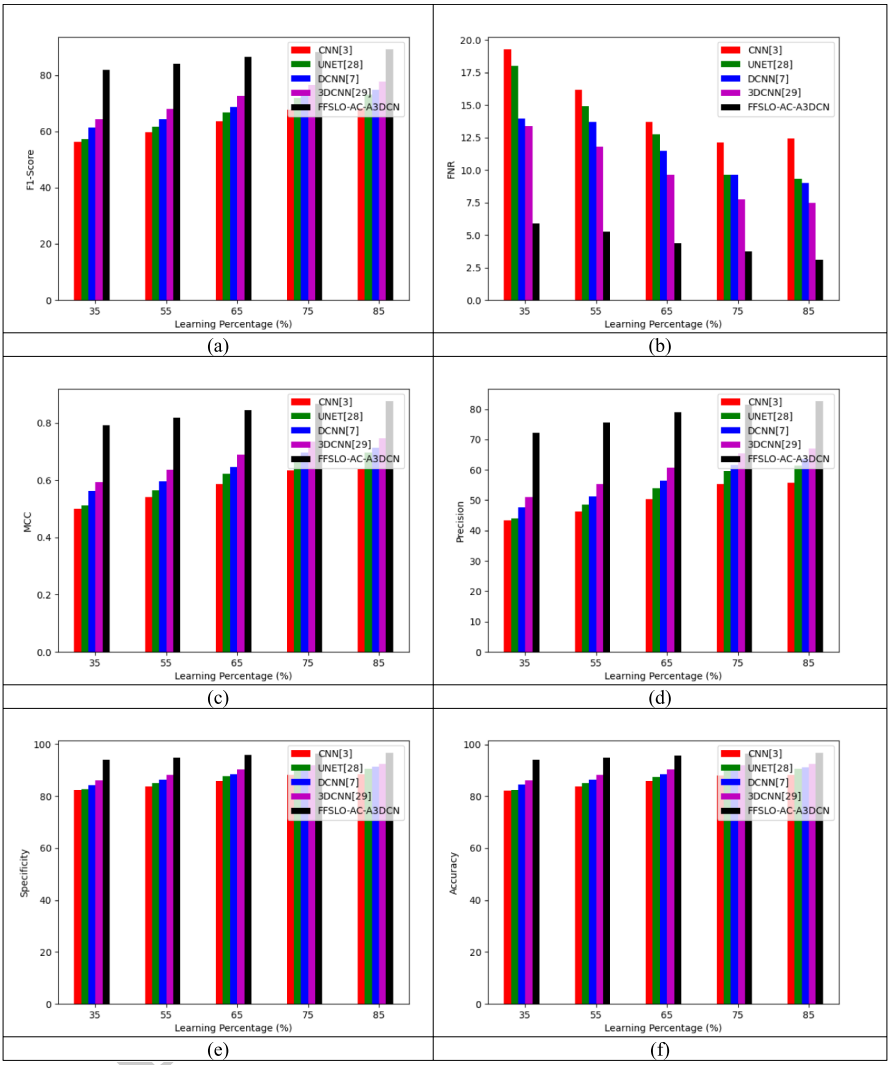

Fig. 3 (continued)

of variance (ANOVA) with repeated metrics. It is utilized to examine differences between groups when the computed dependent variable is ranked in a series. While considering best metrics, the designed model shows 2.61%, 2.05%, 4.86%, and 0.68% elevated than CHOA, CMO, FFOA, and SNOA. Here, the simulation results proved that the developed model is statistically significant. Furthermore, it is illustrated that utilizing HE and CLAHE in the developed approach can improve the contrast and visibility of subtle details in mammogram images.

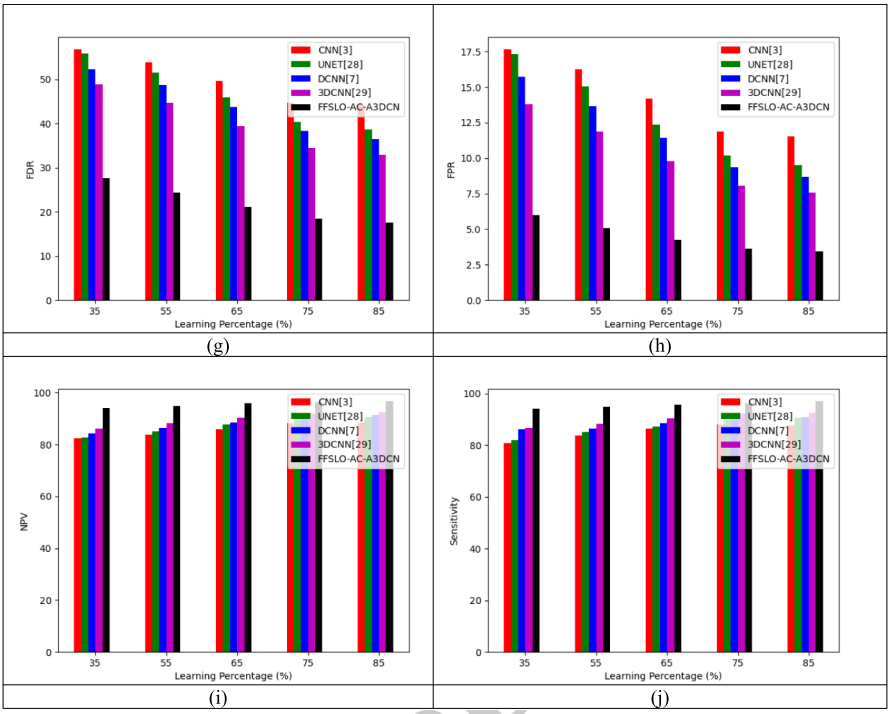

Fig. 3 (continued)

3.8 Convergence Validation of the Designed Framework

The convergence assessment of the suggested framework is signified in Fig. 6. When analyzing the epoch count at 20, the accuracy of the executed model is 20%, 37.14%,12.94%, and 18.51% enhanced than existing methods like CHOA-AC-A3DCNN, CMO-AC-A3DCNN, FFOA-AC-A3DCNN, and SNOA-AC-A3DCNN, respectively. Thus, it is proved that the introduced framework can reduce the time required to reach optimal solutions than other conventional algorithms. The model's effectiveness in quickly achieving convergence not only enhances its practical usability but also positions it as a leading solution for applications demanding immediate results.

3.9 Performance Assessment of the Designed Approach by Varying Dilation Rate

Figure 7 shows the performance analysis of the recommended system. This analysis was carried out by varying the dilation rate to estimate the spatial resolution of the offered framework. Here, the offered approach attained superior performance than the existing approaches. By varying the dilation rate, the introduced system can effectively segment objects and regions of interest in the image. This flexibility

For Appr

in spatial resolution helps the developed model to achieve accurate performance in breast cancer detection. Furthermore, the use of atrous convolution allows the developed model to maintain a consistent computational cost.

3.10 PR-AUC Analysis of the Designed Model

Figure 8 illustrates the precision-recall area under the curve (PR-AUC) analysis on the designed model. This examination helps to effectively estimate the effectiveness of the designed system, particularly when dealing with imbalanced datasets. Here, the graph plots the precision against recall at various classification thresholds. The developed framework achieved a higher Average Precision (AP) value than the other conventional methods like CNN, UNet, DCNN, and 3DCNN. Thus, the outcome illustrated that the introduced method achieves high precision across a wide range of recall levels, indicating better performance in breast cancer detection.

3.11 Sensitivity Evaluation on the Designed Model

Figure 9 shows the sensitivity analysis of the recommended framework. This analysis is performed with respect to key hyper-parameters like dilation rates and learning rates. Here, the dilation rate has a higher impact than the learning rate. Thus, the result demonstrated that the high dilation rate in the offered system can effectively allow the model to capture longer-range dependencies in the image, which can be crucial for image detection tasks.

3.12 ImageNet Comparison on the Introduced Model

Figure 10 depicts the ImageNet comparison of the introduced model. This analysis is carried out by varying the interference time (seconds per image). It allows the researchers to evaluate how well a proposed model balances accuracy with its resource requirements. By analyzing performance on ImageNet, the developed model attained high accuracy with less interference time. The outcome demonstrated that the developed model achieved high accuracy while using less processing time than the existing models.

3.13 Training vs Validation Loss Examination on the Designed Model

Figure 11 shows the training versus validation loss analysis on the developed approach. This analysis was done by varying the epoch count from 1 to 500. This analysis helps the researchers to understand how well the approach is learning the training data and enables them to identify whether the developed model suffers from an overfitting issue. Figure 10 shows that the developed FFSLO algorithm tunes the parameters of the recommended system and it can prevent the overfitting issue.

For Approval

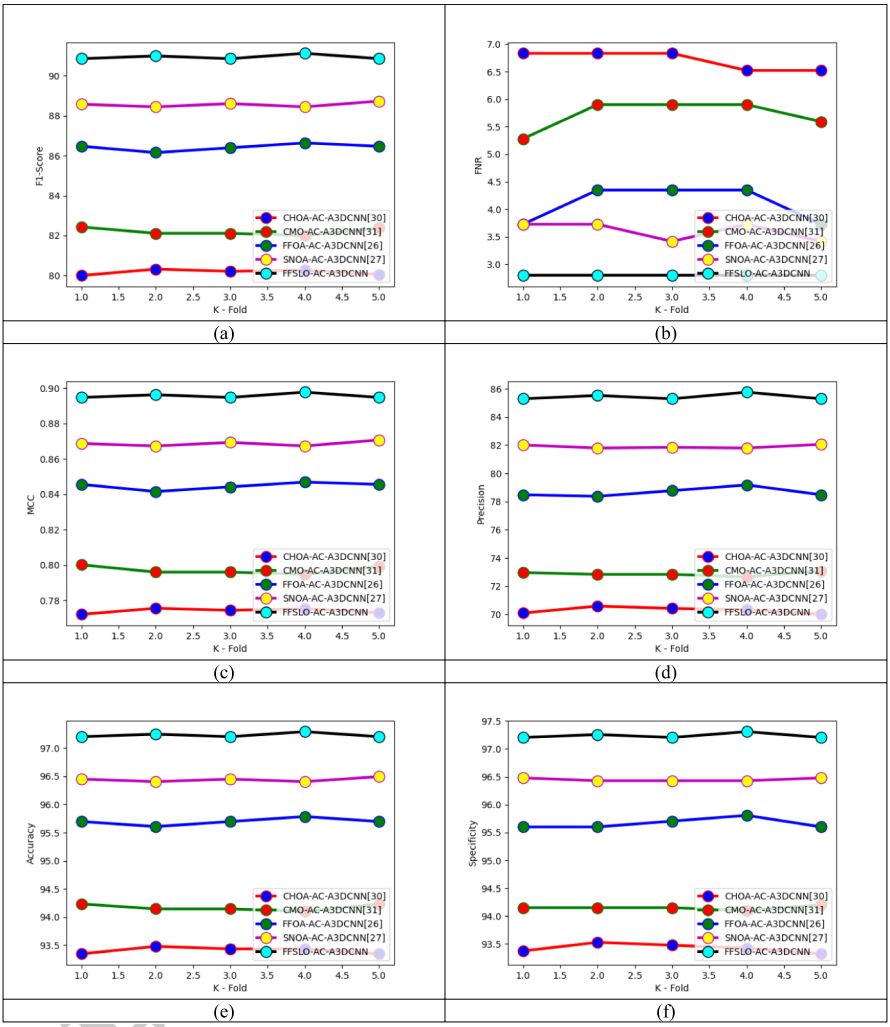

Fig. 4 The K-fold evaluation of the implemented framework over different heuristic algorithms in regards to **a** F1-score; **b** FNR; **c** MCC; **d** precision; **e** accuracy; **f** specificity; **g** sensitivity; **h** FDR; **i** NPV; **j** FPR

3.14 Computational Complexity Investigation on the Designed Model

Table 6 shows the time complexity analysis of the developed system, and Table 7 signifies the space complexity of the designed framework. Here, the duration consumed by the recommended technique is 37.54, which is beneath the other existing models and the optimization algorithms. Thus, the outcome illustrated that the suggested system can effectively detect breast cancer with less computational time and space. The parameter optimization via FFSLO reduces computational complexity and enhances the speed of the detection process. The

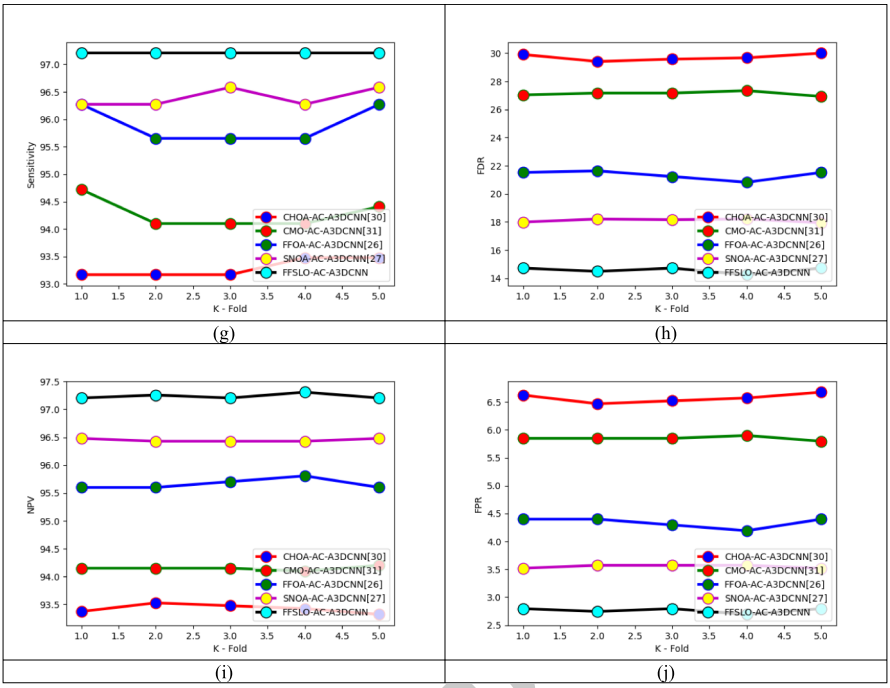

Fig. 4 (continued)

combination of FFOA and SLOA techniques results in faster execution by reducing the computational overhead compared to traditional techniques.

3.15 Visualization of Detection Results on the Designed Model Over State-of-the-Art Methods

Figure 12 shows the visualization of detection results on the introduced model. Here, the F1-score of the developed model was 12.8%, 17.08%, 18.5%, and 23.3% higher than FRNN, GAN, VGG16, and YOLO, respectively. Thus, the experimental outcome showed that the introduced framework accomplished higher effectiveness than the state-of-the-art techniques. Moreover, it is demonstrated that optimizing the parameters of UNet-FCN and AC-A3DCNN using the FFSLO algorithm can effectively identify breast cancer in the early hours.

3.16 Ablation Validation of the Developed Method

The ablation evaluation of the proposed framework is shown in Table 8. This evaluation helps to optimally identify the essential informative features from the gathered mammogram images for improving the system's interpretability. By capturing the important features, it can easily remove the redundancies and unnecessary

For APP

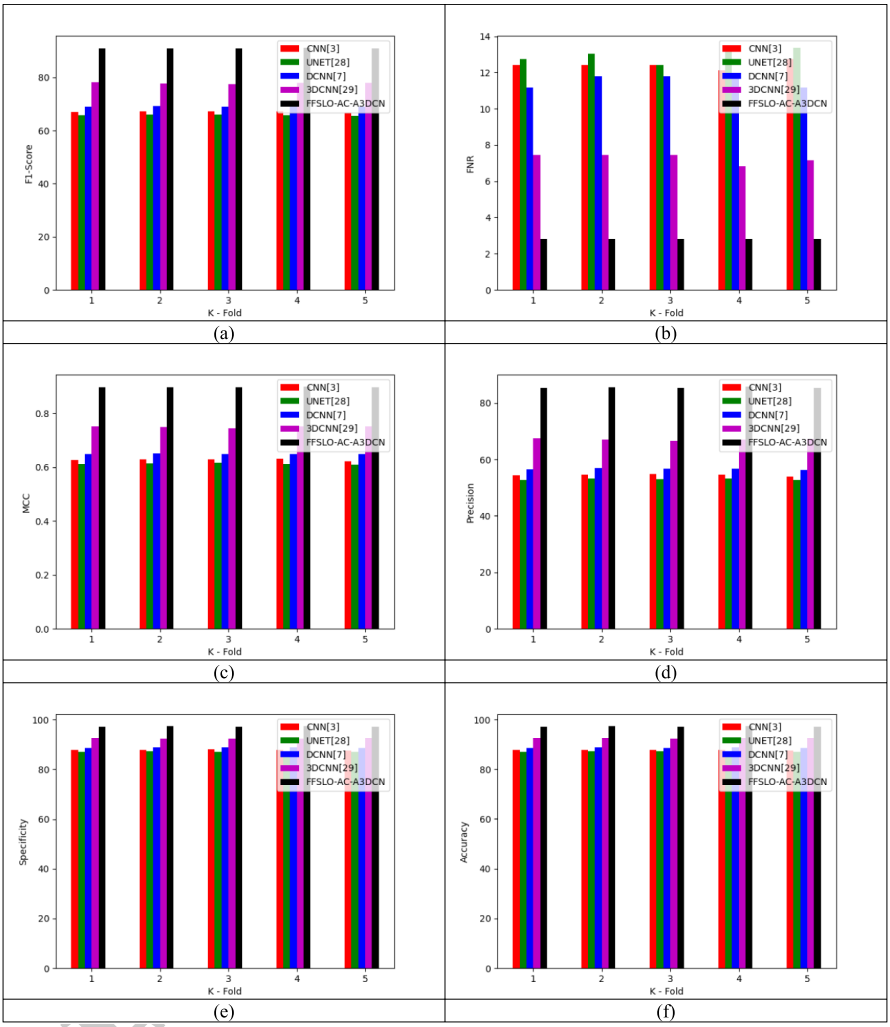

Fig. 5 The K-fold evaluation of the implemented framework over different detection methods in regards to **a** F1-score; **b** FNR; **c** MCC; **d** precision; **e** specificity; **f** accuracy; **g** FDR; **h** FPR; **i** NPV; **j** sensitivity

components in the training process to attain better performance with fewer resources. In Table 8, the traditional attention 3DCNN framework attains a lower sensitivity value of 93.11% to enhance the risk of false negative outcomes. This can incorrectly identify a cancerous condition as non-cancer, leading to a delay in diagnosis and treatment. The higher sensitivity value of 96% is attained by the proposed FFSLO-AC-A3DCNN approach to ensure earlier detection and treatment, and potentially minimize the mortality rates. It helps to prevent breast cancer from progressing to later stages and improve the quality of the patient's life. The FDR error rates of the implemented framework are reduced than 43% dilated 3DCNN, 41% residual 3DCNN, 41% attention 3DCNN, and 22% residual attention AC-3DCNN

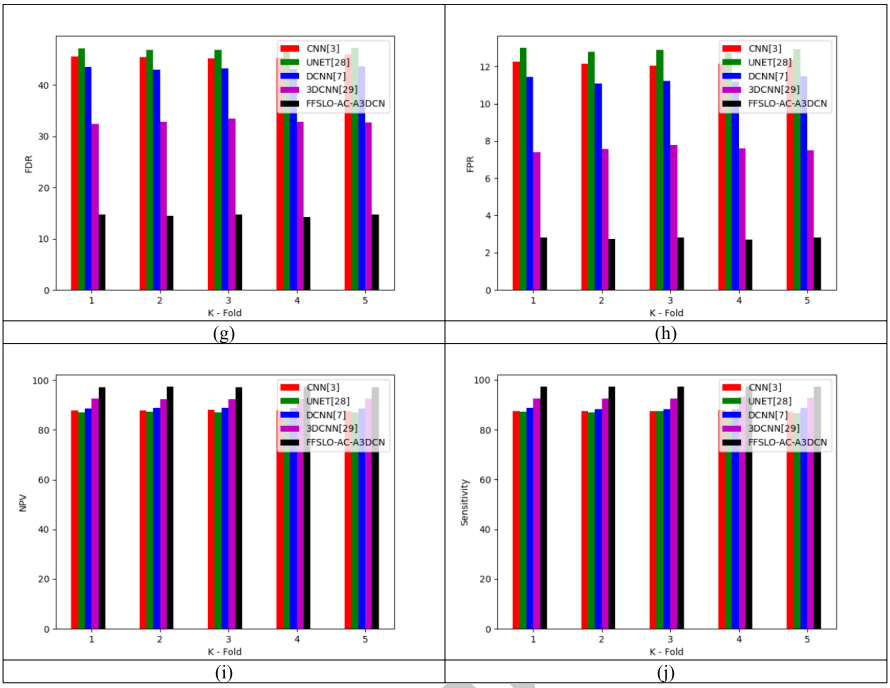

Fig. 5 (continued)

approaches. The developed method has a minimal error rate to enable better accuracy and early detection. Thus, the overall outcomes prove the proposed method's superior performance than the conventional methods.

3.17 Confusion Matrix Evaluation of the Developed Method

Figure 13 displays the confusion matrix validation of the proposed approach with two different datasets. It can easily identify the specific false positives and false negative values to enable better precision. It has the ability to optimally handle vast amounts of sensitive medical mammogram images by reducing the overfitting issues for enhancing better diagnosis within a limited duration. Also, it can provide clear and easy-to-understand visualization of the outcomes. Furthermore, it can analyze the overall features in the gathered medical images and categorize the most informative features to enhance the entire performance in an effective manner. This validation can optimally analyze and identify the several types of errors and misclassification outcomes for effectively categorizing the cancerous and non-cancerous cases. The prescribed hyperparameter tuning process is easily validated by minimizing the overfitting issues. Furthermore, it reduces the misclassified outcomes and ensures the optimal results to enhance the model's generalizability and adaptability.

For App

Table 1 Effective analysis of the implemented model with different existing optimization algorithms and classifiers for dataset 1

Measures	CHOA-AC-A3DCNN[54]	CMO-AC-A3DCNN[55]	FFOA-AC-A3DCNN [45]	SNOA-AC-A3DCNN [46]	FFSLO-AC-A3DCNN
Optimization algorithms					
Accuracy	91.08252	90.81633	93.38953	92.90151	96.62822
Sensitivity	90.99379	90.68323	93.1677	92.54658	96.89441
Specificity	91.09731	90.83851	93.4265	92.96066	96.58385
Precision	63.01075	62.26013	70.25761	68.66359	82.53968
FPR	8.902692	9.161491	6.573499	7.039337	3.416149
FNR	9.006211	9.31677	6.832298	7.453416	3.10559
NPV	91.09731	90.83851	93.4265	92.96066	96.58385
FDR	36.98925	37.73987	29.74239	31.33641	17.46032
F1-score	74.45997	73.83059	80.10681	78.83598	89.14286
MCC	0.709898	0.702748	0.773281	0.758846	0.875548
Classifiers					
Measures	CNN- AC-A3DCNN [21]	UNET- AC-A3DCNN [47]	DCNN- AC-A3DCNN [25]	3DCNN- AC-A3DCNN [53]	FFSLO-AC-A3DCNN
Accuracy	88.33185	90.50577	91.25998	92.45785	96.62822
Sensitivity	87.57764	90.68323	90.99379	92.54658	96.89441
Specificity	88.45756	90.47619	91.30435	92.44306	96.58385
Precision	55.84158	61.34454	63.55748	67.11712	82.53968
FPR	11.54244	9.52381	8.695652	7.556936	3.416149
FNR	12.42236	9.31677	9.006211	7.453416	3.10559
NPV	88.45756	90.47619	91.30435	92.44306	96.58385
FDR	44.15842	38.65546	36.44252	32.88288	17.46032
F1-score	68.19831	73.18296	74.84036	77.80679	89.14286
MCC	0.638125	0.695827	0.713972	0.747768	0.875548

For Approval

Table 2 Effective analysis of the implemented model with different cancer detection classifiers and optimization algorithms for dataset 2

Measures	CHOA-AC-A3DCNN [54]	CMO-AC-A3DCNN [55]	FFOA-AC-A3DCNN [45]	SNOA-AC-A3DCNN [46]	FFSLO-AC-A3DCNN
Optimization algorithms					
Accuracy	92.81278	93.07897	93.87755	94.89796	96.89441
Sensitivity	92.54658	93.1677	93.78882	94.7205	96.89441
Specificity	92.85714	93.06418	93.89234	94.92754	96.89441
Precision	68.34862	69.12442	71.90476	75.68238	83.87097
FPR	7.142857	6.935818	6.10766	5.072464	3.10559
FNR	7.453416	6.832298	6.21118	5.279503	3.10559
NPV	92.85714	93.06418	93.89234	94.92754	96.89441
FDR	31.65138	30.87558	28.09524	24.31762	16.12903
F1-score	78.62797	79.36508	81.40162	84.13793	89.91354
MCC	0.756603	0.765277	0.787977	0.818684	0.8841
Classifiers					
Measures	CNN-AC-A3DCNN [21]	UNET-AC-A3DCNN [47]	DCNN-AC-A3DCNN [25]	3DCNN-AC-A3DCNN [53]	FFSLO-AC-A3DCNN
Accuracy	90.19521	91.34871	92.32476	93.65572	96.89441
Sensitivity	90.68323	90.99379	92.23602	93.47826	96.89441
Specificity	90.11387	91.40787	92.33954	93.6853	96.89441
Precision	60.45549	63.83442	66.74157	71.15839	83.87097
FPR	9.886128	8.592133	7.660455	6.3147	3.10559
FNR	9.31677	9.006211	7.763975	6.521739	3.10559
NPV	90.11387	91.40787	92.33954	93.6853	96.89441
FDR	39.54451	36.16558	33.25843	28.84161	16.12903
F1-score	72.54658	75.03201	77.44459	80.80537	89.91354
MCC	0.68904	0.716026	0.743493	0.781182	0.8841

For Approval

Table 3 Validation of implemented breast cancer detection model using recent approaches

Measures	ConvNet-24 [56]	CNN-SVM [57]	CDCNNs [58]	FFSLO-AC-A3DCNN
Accuracy	93.17	93.52	94.45	96.63
Sensitivity	92.86	93.48	94.72	96.89
Specificity	93.22	93.53	94.41	96.58
Precision	69.53	70.66	73.85	82.54
FPR	6.78	6.47	5.59	3.42
FNR	7.14	6.52	5.28	3.11
NPV	93.22	93.53	94.41	96.58
FDR	30.47	29.34	26.15	17.46
F1-score	79.52	80.48	82.99	89.14
MCC	76.66	77.77	80.62	87.55

Table 4 Statistical validation of the implemented system using the Friedman aligned ranks test

Algorithm comparison	Statistic	Adjusted *p*-value	Result
CHOA vs FFSLO-AC-A3DCNN	1.78885	0.73638	H0 is accepted
FFOA vs CHOA	1.34164	1	H0 is accepted
FFOA vs SNOA	0.44721	1	H0 is accepted
CHOA vs FFSLO-AC-A3DCNN	1.78885	0.73638	H0 is accepted
CMO vs FFSLO-AC-A3DCNN	1.34164	1	H0 is accepted
FFOA vs CMO	0.89443	1	H0 is accepted
CHOA vs SNOA	0.89443	1	H0 is accepted
FFSLO-AC-A3DCNN vs SNOA	0.89443	1	H0 is accepted
FFOA vs FFSLO-AC-A3DCNN	0.44721	1	H0 is accepted
CMO vs CHOA	0.44721	1	H0 is accepted
CMO vs SNOA	0.44721	1	H0 is accepted

Table 5 Statistical validation of the implemented breast cancer detection model using standard metrics

Algorithms	CHOA [54]	CMO [55]	FFOA [45]	SNOA [46]	FFSLO-AC-A3DCNN
Mean	1.134126	1.062407	1.096654	1.074478	1.061372
Median	1.068044	1.061989	1.093273	1.065657	1.053857
Standard deviation	0.093843	0.002922	0.003974	0.042277	0.035607
Worst	1.340675	1.082863	1.101324	1.239686	1.199023
Best	1.068044	1.061989	1.093273	1.047263	1.040116

4 Discussion

The work concentrates on validating the outcomes with diverse efficacy metrics for achieving efficient performance. In Fig. 4, performance analysis was done on the developed model over different techniques and algorithms. Here, the introduced model's

For Approval

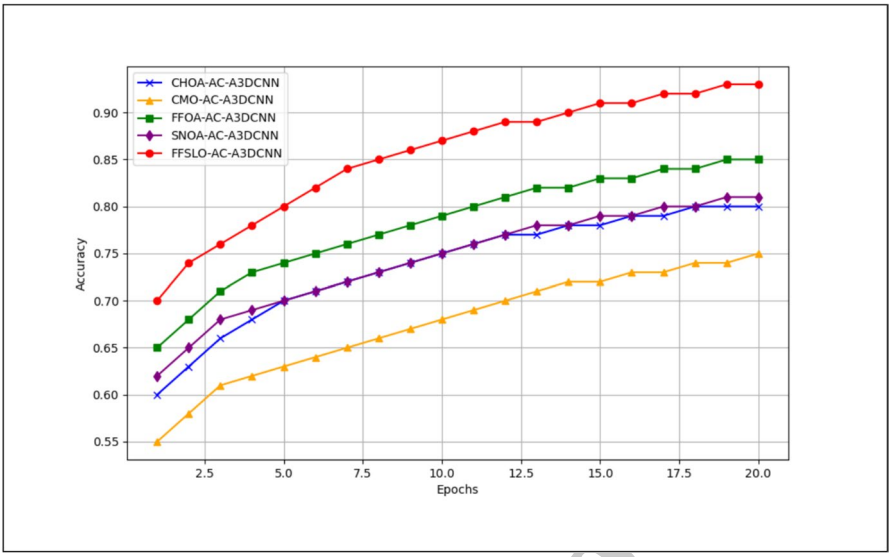

Fig. 6 Convergence analysis of the offered model

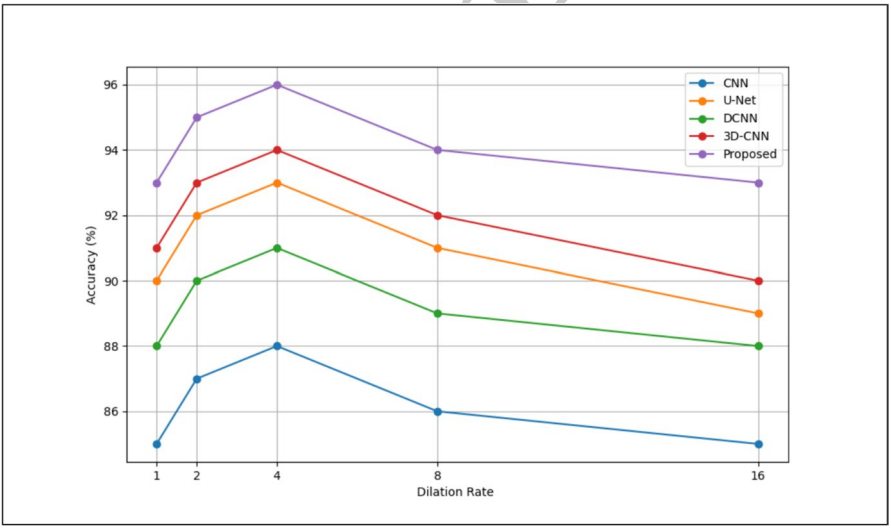

Fig. 7 Performance analysis of the suggested model by varying dilation rate

accuracy is 18.07% enhanced than CNN, 20.9% greater than UNET, 17% superior to DCNN, and 15% better than 3DCNN. Thus, this analysis showed that the developed model accurately detects breast cancer than other existing approaches. Furthermore, k-fold analysis was performed on the suggested framework and it was shown in Figs. 4 and 5. Here, F1-score of the introduced model was 23.12%, 19.39%, 13.21%, and 11.2%

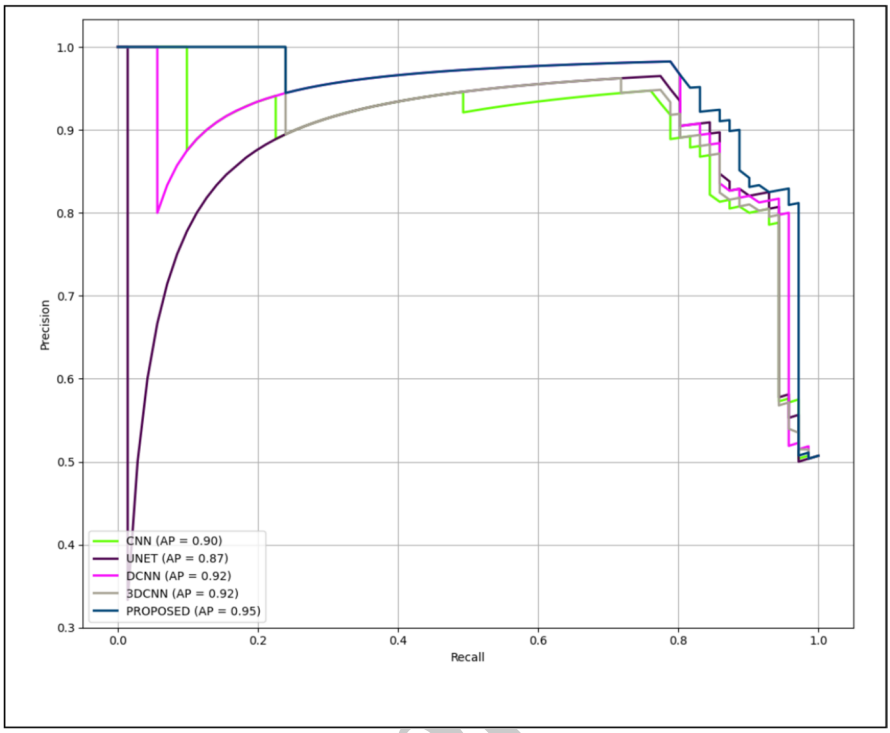

Fig. 8 PR-AUC analysis of the suggested model

enhanced than CHOA-AC-A3DCNN, CMO-AC-A3DCNN, FFOA-AC-A3DCNN, and SNOA-AC-A3DCNN cancer detection models. Additionally, overall analysis was performed in Tables 1 and 2 to display the performance of the offered model. Here, the precision of the proposed model was 82.53%, which is enhanced than the conventional approaches. Moreover, statistical analysis is validated on the suggested framework and it is shown in Tables 4 and 5. Here, the FFSLO-AC-A3DCNN approach attained better performance than the CHOA, CMO, FFOA, and SNOA, respectively. While considering accuracy, the existing CMO-AC-A3DCNN model shows 90%, which shows lower performance than the other techniques. From the entire validation, the designed model gives enhanced performance than the conventional techniques in breast cancer detection.

Clinical Applicability of the Proposed Model In real-world clinical use, healthcare professionals use the designed model. It allows healthcare professionals to identify subtle abnormalities in imaging data more readily. It can improve the accuracy of breast tumor diagnosis by segmenting and detecting breast tissue abnormalities on mammograms. This may lead to earlier detection, improved treatment options, and better patient outcomes. Moreover, the developed model is most applicable within clinical settings where medical imaging like mammograms are used for breast

FOR API

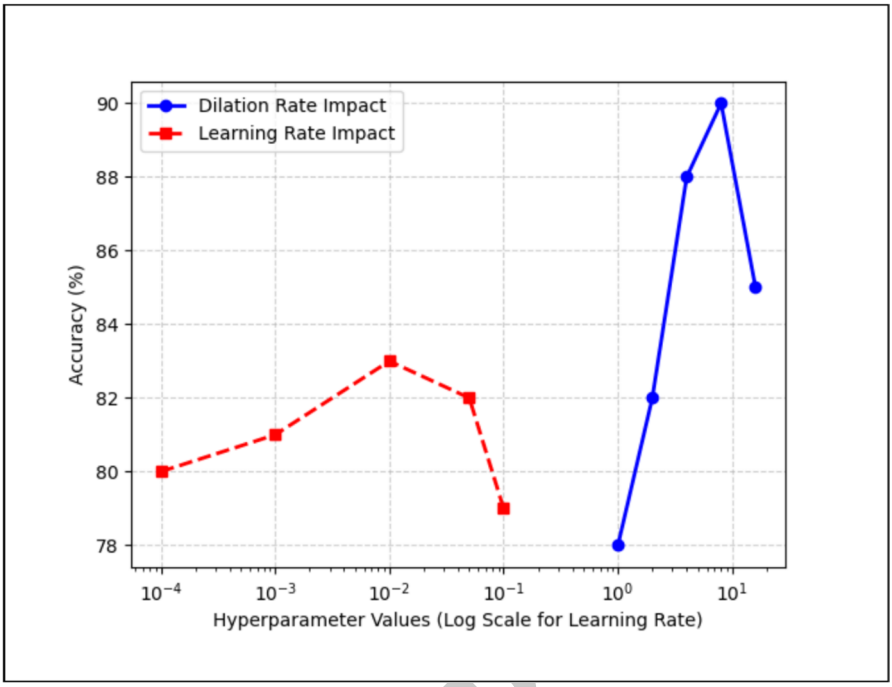

Fig. 9 Sensitivity examination of the designed model

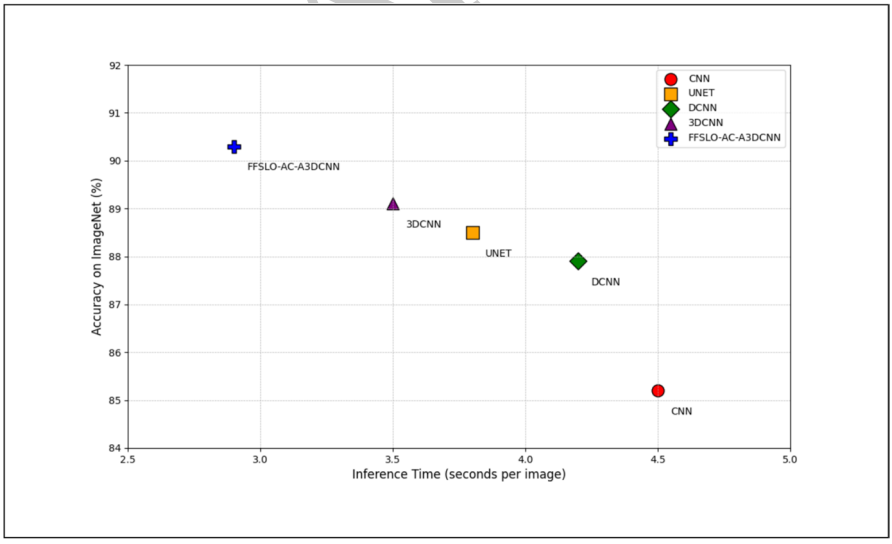

Fig. 10 ImageNet comparison of the proposed framework

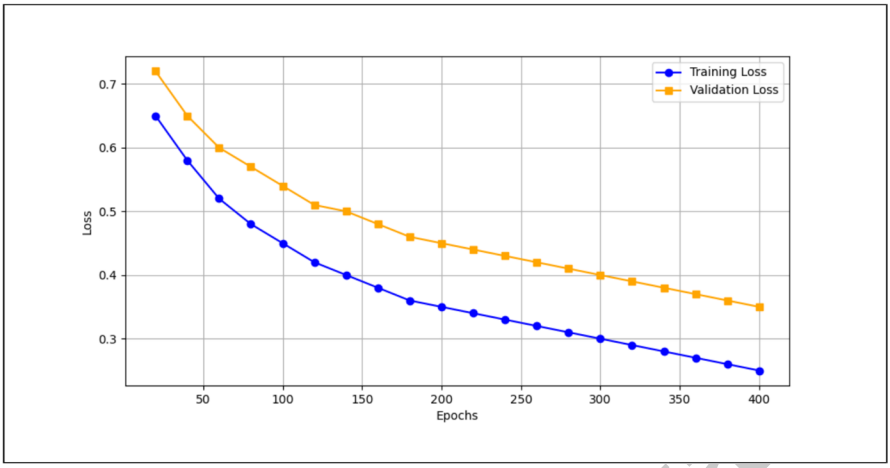

Fig. 11 Training vs validation loss analysis on the developed approach

Table 6 Time complexity analysis of the designed framework

Terms	Time (min)
Optimization algorithms	
CHOA [54]	41.4733
CMO [55]	49.8542
FFOA [45]	42.5332
SNOA [46]	45.2277
FFSLO-AC-A3DCNN	37.5428
Techniques	
CNN [21]	50.854
UNET [47]	49.4673
DCNN [25]	51.9544
3DCNN [53]	52.8647
FFSLO-AC-A3DCNN	37.5428

Table 7 Space complexity analysis of the introduced framework

Algorithm	Complexity
CHOA [54]	$O(iter * (2nop * chlen + 3))$ Here, the term $iter$ denotes the number of iterations, nop signifies the number of populations and $chlen$ denotes the chromosome length
CMO [55]	$O(iter * (2nop + 3+ * chlen + 1))$
FFOA [45]	$O(iter * ((nop * 2chlen) + (nop * 2chlen)))$
SNOA [46]	$O(iter * (nop * 2chlen + 3))$
FFSLO-AC-A3DCNN	$O(iter * (nop * 2chlen + 1))$

For Approval

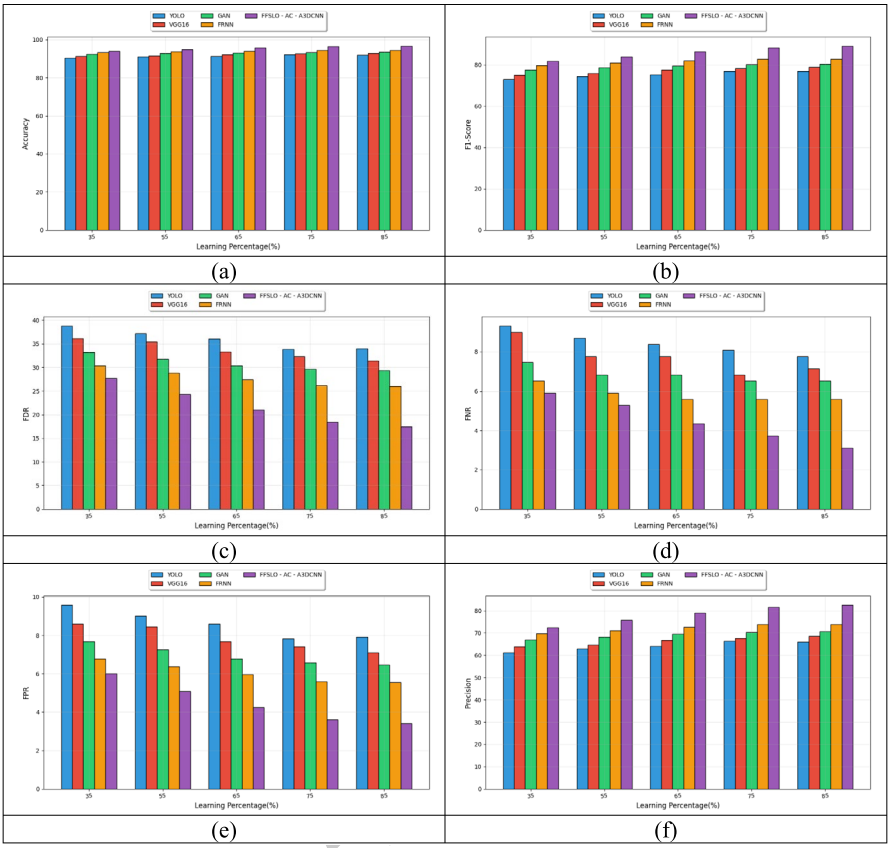

Fig. 12 Visualization of detection results on the introduced framework based on **a** accuracy, **b** F1-score, **c** FDR, **d** FNR, **e** FPR, and **f** precision

Table 8 Ablation study of the proposed framework

Measures/methods	Dilated 3DCNN	Residual 3DCNN	Attention 3DCNN	Residual attention AC-3DCNN	Proposed FFSLO-AC-A3DCNN
Accuracy	93.17	93.35	93.39	95.43	96.63
Sensitivity	93.48	93.17	93.11	95.65	96.89
Specificity	93.12	93.37	93.43	95.39	96.58
Precision	69.35	70.09	70.26	77.58	82.54
FPR	6.88	6.63	6.57	4.61	3.42
FNR	6.52	6.83	6.83	4.35	3.11
NPV	93.12	93.37	93.43	95.39	96.58
FDR	30.65	29.91	29.74	22.42	17.46
F1-score	79.63	80.00	80.11	85.67	89.14
MCC	76.85	77.21	77.33	83.64	87.55

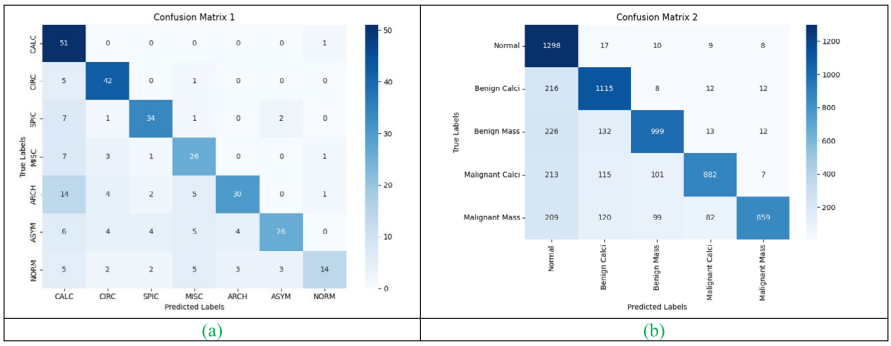

Fig. 13 Confusion matrix evaluation of the developed method based on **a** dataset 1 and **b** dataset 2

cancer screening. This allows the proposed model to assist radiologists in identifying suspicious areas and potentially detecting cancers at earlier stages, especially in situations where there might be a high volume of complex breast tissue densities, and helps to speed up the diagnosis process in breast cancer.

5 Conclusion

The newly developed deep-learning-based FFSLO-AC-A3DCNN breast cancer detection model was used to detect changes in the selected images. These images are taken from online resources. In the first step, the collected data was pre-processed using strategies like HE and CLAHE. In the implemented FFSLO-AC-A3DCNN, the best features were chosen from the final pre-processed data. Next, images were given to the segmented area. Here, the combination of UNet and FCN techniques is used in the segmentation process, and they obtained the UNet-based segmented images and FCN-based segmented images. Then averaging the UNet segmented and FCN segmented images improved the breast cancer detection system's accuracy. The outcome illustrated that the developed system performed better accuracy when compared to the other methods. The created FFSLO-AC-A3DCNN-based breast cancer detection model outperformed the detection approaches CNN, UNet, DCNN, and 3DCNN with precision of 47.7%, 34.5%, 29.8%, and 22.9%, respectively. As a result, the assessment findings of the breast cancer detection model put into practice showed that it performed better and produced more effective results than the recently used techniques. In the future, the transfer learning technique will be included with diverse image datasets to improve the detection accuracy. In addition, we will improve the offered approach by using diverse angles of mammography images. Furthermore, we will use the grid search to find the best combination of hyperparameters for a developed model. Also, the upcoming work will focus on using the SHapley Additive exPlanations (SHAP) or local interpretable model-agnostic explanations method (LIME) to trade off between accuracy and interpretability in breast cancer detection.

For Approval

Acknowledgements I would like to express my very great appreciation to the co-authors of this manuscript for their valuable and constructive suggestions during the planning and development of this research work.

Author Contribution All authors have made substantial contributions to conception and design, revising the manuscript, and the final approval of the version to be published. Also, all authors agreed to be accountable for all aspects of the work in ensuring that questions related to the accuracy or integrity of any part of the work are appropriately investigated and resolved.

Data Availability No datasets were generated or analysed during the current study.

Ethics Approval Not applicable.

Informed Consent Not applicable.

Competing interests The authors declare no competing interests.

For Approval

References

1. Lee J, Nishikawa RM (2022) Identifying women with mammographically- occult breast cancer leveraging GAN-simulated mammograms. IEEE Trans Med Imaging 41:225–236
2. Azour F, Boukerche A (2022) Design guidelines for mammogram-based computer-aided systems using deep learning techniques. IEEE Access 10:21701–21726
3. Gao M, Fessler JA, Chan HP (2021) Deep convolutional neural network with adversarial training for denoising digital breast tomosynthesis images. IEEE Trans Med Imaging 40:1805–1816
4. Li H, Chen D, Nailon WH, Davies ME, Laurenson DI (2022) Dual convolutional neural networks for breast mass segmentation and diagnosis in mammography. IEEE Trans Med Imaging 41:3–13
5. Beeravolu AR, Azam S, Jonkman M, Shanmugam B, Kannoorpatti K, Anwar A (2021) Preprocessing of breast cancer images to create datasets for deep-CNN. IEEE Access 9:33438–33463
6. Shu X, Zhang L, Wang Z, Lv Q, Yi Z (2020) Deep neural networks with region-based pooling structures for mammographic image classification. IEEE Trans Med Imaging 39:2246–2255
7. Toz G, Erdoğmuş P (2021) A novel hybrid image segmentation method for detection of suspicious regions in mammograms based on adaptive multi-thresholding (HCOW). IEEE Access 9:85377–85391
8. Ganesan K, Acharya UR, Chua CK, Min LC, Abraham KT, Ng KH (2013) Computer-aided breast cancer detection using mammograms: a review. IEEE Rev Biomed Eng 6:77–98
9. Heidari M, Lakshmivarahan S, Mirniaharikandehei S (2021) Applying a random projection algorithm to optimize machine learning model for breast lesion classification. IEEE Trans Biomed Eng 68:2764–2775
10. El-Naqa I, Yongyi Y, Wernick MN, Galatsanos NP, Nishikawa R (2002) Support vector machine learning for detection of microcalcifications in mammograms. In: Proceedings IEEE International Symposium on Biomedical Imaging. IEEE, pp 201–204
11. Kaur M, Khullar V, Singh HP (2020) Transfer learning for breast cancer classification using small dataset of ultrasound images. In: 2020 3rd International Conference on Intelligent Sustainable Systems (ICISS). IEEE, pp 1050–1056
12. Malebary SJ, Hashmi A (2021) Automated breast mass classification system using deep learning and ensemble learning in digital mammogram. IEEE Access 9:55312–55328
13. Wei L, Yang Y, Nishikawa RM, Wernick MN, Edwards A (2005) Relevance vector machine for automatic detection of clustered microcalcifications. IEEE Trans Med Imaging 24:1278–1285
14. Liu W, Shu X, Zhang L, Li D, Lv Q (2022) Deep multiscale multi-instance networks with regional scoring for mammogram classification. IEEE IEEE Trans Artif Intell 3:485–496
15. Song R, Li T, Wang Y (2020) Mammographic classification based on XGBoost and DCNN with multi features. IEEE Access 8:75011–75021

16. Hao D, Zhang L, Sumkin J, Mohamed A, Wu S (2020) Inaccurate labels in weakly-supervised deep learning: automatic identification and correction and their impact on classification performance. IEEE J Biomed Health Inf 24:2701–2710
17. Singh S, Bovis K (2005) An evaluation of contrast enhancement techniques for mammographic breast masses. IEEE Trans Inf Technol Biomed 9:109–119
18. Patil R, Biradar N, Pawar R (2022) A new automated segmentation and classification of mammogram images. Multimedia Tools Appl 81:7783–7816
19. Su Y, Liu Q, Xie W, Hu P (2022) YOLO-LOGO: a transformer-based YOLO segmentation model for breast mass detection and segmentation in digital mammograms. Comput Methods Programs Biomed 221:106903
20. Punithavathi V, Devakumari D (2021) WITHDRAWN: a new proposal for the segmentation of breast lesion in mammogram images using optimized kernel fuzzy clustering algorithm
21. Keshk A, Saber A, Sakr M, Abo-Seida OM, Chen H (2021) A novel deep-learning model for automatic detection and classification of breast cancer using the transfer-learning technique. IEEE Access 9:71194–71209
22. Cascio D, Fauci F, Magro R, Raso G, Bellotti R (2006) Mammogram segmentation by contour searching and mass lesions classification with neural network. IEEE Trans Nucl Sci 53:2827–2833
23. Shen T, Gou C, Wang J, Wang FY (2020) Simultaneous segmentation and classification of mass region from mammograms using a mixed-supervision guided deep model. IEEE Signal Process Lett 27:196–200
24. Singh VK, Rashwan HA, Romani S, Akram F, Pandey N, Sarker MK, Saleh A, Arenas M, Arquez M, Puig D, Barrena JT (2020) Breast tumor segmentation and shape classification in mammograms using generative adversarial and convolutional neural network. Expert Syst Appl 139:112855
25. Nagalakshmi, T (2022) Breast cancer semantic segmentation for accurate breast cancer detection with an ensemble deep neural network. Neural Process Lett 54(6):5185–5198
26. Punitha M, Perumal K (2019) Hybrid segmentation and feature extraction approach to detect tumour based on fuzzy rough-in mammogram images. Procedia Comput Sci 165:478–484
27. Mahmood T (2024) RehmanA, SabaT, WangY, AlamriF S, Alzheimer's disease unveiled: cutting-edge multi-modal neuroimaging and computational methods for enhanced diagnosis. Biomed Signal Proces Control 97:106721
28. ArshadW MasoodT (2023) MahmoodT, JaffarA, AlamriF S, BahajSA O, KhanA R, Cancer unveiled: a deep dive into breast tumor detection using cutting-edge deep learning models, *IEEE*. Access 11:133804–133824
29. Mahmood T, Rehman A, Saba T, Nadeem L, Bahaj SAO (2023) Recent advancements and future prospects in active deep learning for medical image segmentation and classification. IEEE Access 11:13623–113652
30. Mahmood T (2021) LiJ, PeiY, AkhtarF. An automated in-depth feature learning algorithm for breast abnormality prognosis and robust characterization from mammography images using deep transfer learning. Biology 10(9):859
31. Mahmood T, Li J, Pei Y, Akhtar F, Rehman MU, Wasti SH (2022) Breast lesions classifications of mammographic images using a deep convolutional neural network-based approach. Plos one 17(1):e0263126
32. Mahmood T (2024) SabaT. RehmanA, AlamriF S, Harnessing the power of radiomics and deep learning for improved breast cancer diagnosis with multiparametric breast mammography, Expert Syst, Appl 249:123747
33. Mahmood T, Li J, Pei Y, Akhtar F, Imran A, Rehman KU (2020) A brief survey on breast cancer diagnostic with deep learning schemes using multi-image modalities. IEEe Access 8 :165779–165809
34. PandeyS K (2023) ShuklaA. BhatiaS, GadekalluT R, KumarA, MashatA, ShahM A, JanghelR R, Detection of arrhythmia heartbeats from ECG signal using wavelet transform-based CNN model, International Journal of Computational Intelligence Systems 16:80
35. Venu DN (2023) PSNR based evalution of spatial Guassian kernals for FCM algorithm with mean and median filtering based denoising for MRI segmentation. IJFANS International Journal of Food and Nutritional Sciences 12:928–939
36. Vasu GT (2023) PalanisamyP, Gradient-based multi-focus image fusion using foreground and background pattern recognition with weighted anisotropic diffusion filter. Sig Imag Video Process 17:2531–2543

Under Approval

37. Vijayalakshmi D, Nath MK (2023) A strategic approach towards contrast enhancement by two-dimensional histogram equalization based on total variational decomposition. Multimed Tools Appl 82(13):19247–19274
38. Sunaryo M, Hariadi M (2016) Preprocessing on digital image using histogram equalization: an experiment study on MRI brain image. International Journal of Computer Science and Information Technologies 7:1723–1727
39. Vijayalakshmi D (2022) Malaya Kumar Nath, A novel multilevel framework based contrast enhancement for uniform and non-uniform background images using a suitable histogram equalization. Digital Signal Processing 127:103532
40. Chaudhury S, Krishna AN, Gupta S, Sankaran KS, Khan S, Sau K, Raghuvanshi A, Sammy F (2022) [Retracted] Effective image processing and segmentation-based machine learning techniques for diagnosis of breast cancer. Comput Math Methods Med 2022(1):6841334
41. Kumar A (2024) DhankaS. SinghJ, KhanAA, MainiS, Hybrid machine learning techniques based on genetic algorithm for heart disease detection, Innovation and Emerging Technologies 11:2450008
42. Albadr MAA, Ayob M, Tiun S, Homod RZ, AL-Dhief FT, Mutar MH (2024) Parkinson's disease diagnosis by voice data using particle swarm optimization-extreme learning machine approach. Multimed Tools Appl 1–34
43. Madlool ZA (2024) Develop whale optimization algorithm (WOA) in genetic method to predict the optimal treatment for diseases. Journal of Al-Qadisiyah for Computer Science and Mathematics 16:300–310
44. Xia B (2024) InnabN. KandasamyV, AhmadianA, FerraraM, Intelligent cardiovascular disease diagnosis using deep learning enhanced neural network with ant colony optimization, Scientific Reports 14:21777
45. Shayanfar H, Soleimanian F, Chopogh G (2018) Farmland fertility: a new metaheuristic algorithm for solving continuous optimization problems. Appl Soft Comput 71:728–746
46. Coufal P, Hubálovský Š, Hubálovská M, Balogh Z (2021) Snow leopard optimization algorithm: a new nature based optimization algorithm for solving optimization problems. Math 9(21):2832
47. Guo Y, Duan X, Wang C, Guo H (2021) Segmentation and recognition of breast ultrasound images based on an expanded U-Net. Plos one 16(6):e0253202
48. Balasubramanian PK (2023) LaiWC. SengG H, SelvarajJ, Apestnet with mask r-cnn for liver tumor segmentation and classification, Cancers 15(2):330
49. GabA AM, SarhanA M, ElshennawyN M (2023) Edge U-Net: brain tumor segmentation using MRI based on deep U-Net model with boundary information. Expert Syst Appl 213:118833
50. Mujtaba G, Ahmad J (2024) UAV-based road traffic monitoring via FCN segmentation and deepsort for smart cities. ICIC
51. Nallasivan G (2023) RamachandranV, AlroobaeaR, AlmotiriJ, Liver tumors segmentation using 3D SegNet deep learning approach. Comput Syst Sci Eng 45:1655–1677
52. Liu Q (2023) ZhangY, ChenJ, SunC, HuangM, CheM, LiC, LinS, An improved Deeplab V3+ network based coconut CT image segmentation method. Front Plant Sci 14:1139666
53. Vrskova R, Hudec R, Kamencay P, Sykora P (2022) Human activity classification using the 3DCNN architecture. Appl Sci 12(2):931
54. Moharam R, Ali AF, Morsy E, Ahmed MA, Mostafa MSM (2022) A discrete chimp optimization algorithm for minimizing tardy/lost penalties on a single machine scheduling problem. IEEE Access 10:52126–52138
55. Zhou D, Wang J, Jiang B, Guo H, Li Y (2018) Multi-task multi-view learning based on cooperative multi-objective optimization. IEEE Access 6:19465–19477
56. Poonguzhali Elangovan D (2024) Vijayalakshmi & Malaya Kumar Nath, COVID-19Net: an effective and robust approach for COVID-19 detection using ensemble of ConvNet-24 and customized pre-trained models. Circuits Systems Signal Process 43:2385–2408
57. Keerthana D, Venugopal V (2023) Malaya Kumar Nath, Madhusudhan Mishra, Hybrid convolutional neural networks with SVM classifier for classification of skin cancer, *Biomedical*. Eng Adv 5:100069
58. Vijayalakshmi D, Elangovan P, Nath MK (2024) Methodology for improving deep learning-based classification for CT scan COVID-19 images. Biomed Eng: Appl Basis Commun 36(03):2450008

Publisher's Note Springer Nature remains neutral with regard to jurisdictional claims in published maps and institutional affiliations.

For Approval

Springer Nature or its licensor (e.g. a society or other partner) holds exclusive rights to this article under a publishing agreement with the author(s) or other rightsholder(s); author self-archiving of the accepted manuscript version of this article is solely governed by the terms of such publishing agreement and applicable law.

Authors and Affiliations

Rashmi V Pawar[1] · Rajashekhargouda C. Patil[2] · Rajeshwari S. Patil[3] · Ambaji S. Jadhav[1]

✉ Rashmi V Pawar
rashmi.ajadhav@gmail.com

Rajashekhargouda C. Patil
patilrajuc@gmail.com

Rajeshwari S. Patil
rspatil1272014@gmail.com

Ambaji S. Jadhav
asjadhavec@gmail.com

[1] Department of Electrical and Electronics, Affiliated to Visvesvaraya Technological University Belagavi, Karnataka, India, BLDEA's V.P. Dr. P.G. Halakatti College of Engineering and Technology, Adarsh Nagar, Vijayapura, Karnataka 586103, India

[2] Department of Electronics and Communication Engineering, Affiliated to Visvesvaraya Technological University Belagavi, Karnataka, India, Jain College of Engineering, Machhe, Belagavi, Karnataka 590014, India

[3] Department of Electronics and Communication Engineering, Affiliated to Visvesvaraya Technological University Belagavi, Karnataka, India, BLDEA's V.P. Dr. P.G. Halakatti College of Engineering and Technology, Adarsh Nagar, Vijayapura, Karnataka 586103, India

For Approval